

Nested Deep Learning Model Towards a Foundation Model for Brain Signal Data

Fangyi Wei

Faculty of Business and Economics, The University of Hong Kong, China

Jiajie Mo

Department of Neurosurgery, Beijing Tiantan Hospital, China

Kai Zhang

Department of Neurosurgery, Beijing Tiantan Hospital, China

Haipeng Shen

Faculty of Business and Economics, The University of Hong Kong, China

Srikantan Nagarajan

Department of Radiology, University of California, San Francisco

Fei Jiang*

Department of Epidemiology and Biostatistics,

University of California, San Francisco

October 10, 2024

Abstract

Epilepsy affects over 50 million people globally, with EEG/MEG-based spike detection playing a crucial role in diagnosis and treatment. Manual spike identification is time-consuming and requires specialized training, limiting the number of professionals available to analyze EEG/MEG data. To address this, various algorithmic approaches have been developed. However, current methods face challenges in handling varying channel configurations and in identifying the specific channels where spikes originate. This paper introduces a novel Nested Deep Learning (NDL) framework designed to overcome these limitations. NDL applies a weighted combination of signals across all channels, ensuring adaptability to different channel setups, and allows clinicians to identify key channels more accurately. Through theoretical analysis and empirical validation on real EEG/MEG datasets, NDL demonstrates superior accuracy in spike detection and channel localization compared to traditional methods. The results show that NDL improves prediction accuracy, supports cross-modality data integration, and can be fine-tuned for various neurophysiological applications.

Keywords: epilepsy, EEG, MEG, spike detection, deep learning, neuroimaging.

*Email: fei.jiang@ucsf.edu

1 Introduction

Currently, over 50 million people worldwide live with epilepsy (World Health Organization 2024). Abnormal waveforms, particularly the spikes, detected by Electroencephalography (EEG) during the interictal period play a crucial role in the diagnosis of epilepsy. Spikes are abnormal brain activities measured with EEG or Magnetoencephalography (MEG) devices. They typically occur intermittently and spontaneously, lasting around 0.1–0.25 seconds, and can be observed repeatedly in EEG/MEG recordings. Identifying spikes not only helps predict seizure risk but also assists in localizing the seizure onset zone, which is critical for epilepsy surgery (Smith et al. 2022). It thus becomes imperative to develop novel interpretable methods to effectively identify spikes to assist clinical decision.

The clinical manual identification of spikes is a labor-intensive process, especially when analyzing continuous or video EEG studies that can last over 24 hours. This task requires specialized training, which restricts the number of clinicians qualified to assess EEG studies, resulting in a significant shortage of neurologists proficient in interpreting EEG data (Torres & Butter 1996). To mitigate this issue, various algorithm-based methods have been proposed to automate the identification process. For instance, Baud et al. (2018) utilize an unsupervised learning approach to automate the spike detection. Fukumori et al. (2021) introduce a linear-phase filters for spike detection. With the advancement of deep learning, the field is increasingly adopting deep learning algorithms for the spike detection. For example, Antoniadis et al. (2016), Johansen et al. (2016), Tjepkema-Cloostermans et al. (2018), Thomas et al. (2020), Clarke et al. (2021) and Chung et al. (2023) employ convolutional neural networks (CNNs) to classify abnormal and normal waveforms. Medvedev et al. (2019) use a Long Short-Term Memory neural network for the spike detection task.

However, despite these developments, two significant challenges remain unresolved.

Firstly, the number of channels, their locations, and the montages used vary between studies, making it difficult to develop a universal algorithm that can accommodate all channel setups. For instance, Golmohammadi et al. (2019) develop an algorithm based on the spikes labeled using the temporal central parasagittal montage with 22 channels, whereas Jing et al. (2020)’s algorithm is designed for the longitudinal bipolar montage with 18 channels, and the common average reference montage with 19 channels. Creating a generalized algorithm adaptable to different channel settings is crucial because it allows for the integration of data across studies, thereby enhancing prediction accuracy. Additionally, it enables clinicians to choose their preferred montage for analysis. Secondly, current detection algorithms are limited to identifying the time segment containing a spike but lack the ability to pinpoint the exact channels where the spikes originate. Identifying the specific channels is crucial as it helps locate the seizure onset zone, assists clinicians in reviewing and validating the detection results, and serves as a key factor in ruling out false spike detections that identified on less likely channels.

We propose a novel nested deep learning framework (NDL) to address these challenges. To address the first challenge, we propose a weight function for each channel, customized to its specific signal pattern within a given time range of interest. Then we allow the probability of the time segment containing a spike to be determined by a weighted combination of signals across all channels. For the second challenge, we design these weights to reflect the significance of each channel, providing insight into their importance in the spike detection process. This approach is superior to the traditional channel-based methods (Wilson et al. 1999, Goelz et al. 2000), which require the tedious process of labeling each channel to achieve similar results. NDL offers a faster inference process, enabling it to handle large volumes of data simultaneously. Furthermore, NDL considers the signal information from

all the channels, which improves the prediction accuracy because there are often concurrent spikes that appear on multiple channels. Moreover, because NDL is invariant to channel configurations, it can serve as a foundational model for integrating neurophysiological data from various modalities and can be fine-tuned to adapt to different new tasks.

We propose the model and estimator in Section 2, and present the deep learning estimation procedure in Section 3. Furthermore, we illustrate the theoretical property of the estimator in Section 4. We evaluate NDL on the real data set in Section 5 and some simulated datasets in Section 6.

To facilitate the presentation, we define the following notations. The L_0 , L_1 , L_2 and the supremum norms of vector \mathbf{v} are denoted by $\|\mathbf{v}\|_0$, $\|\mathbf{v}\|_1$, $\|\mathbf{v}\|_2$ and $\|\mathbf{v}\|_\infty$. Furthermore, for a given matrix \mathbf{M} , we denote the matrix entry-wise supremum norm, L_0 , L_1 , operator norms as $\|\mathbf{M}\|_\infty$, $\|\mathbf{M}\|_0$, $\|\mathbf{M}\|_1$, and $\|\mathbf{M}\|_2$. For function $f(\mathbf{x})$, we denote the functional supremum norm as $\|f(\mathbf{x})\|_\infty \equiv \sup |f(\mathbf{x})|$.

2 Model

Let $\mathbf{X}_i = \{\mathbf{X}_{il}, l = 1, \dots, d\}^\top$ be a random matrix representing a multi-channel segment of signals, where \mathbf{X}_{il} is a T -dimensional vector that represents the signal on sensor l , d is the number of sensors, and $T < \infty$. Our goal is to predict whether the i -th segment \mathbf{X}_i contains a spike or not. Additionally, let Y_i be the indicator of the occurrence of a spike in the segment i that appears on a subset of channels. Furthermore, let $\omega_k^*(\mathbf{X}_{il}) : \mathbb{R}^T \rightarrow \mathbb{R}$, $k = 1, \dots, p$ be a scalar function of \mathbf{X}_{il} , and define $\alpha_k^*(\mathbf{X}_{il}, \mathbf{X}_i) = \exp\{\omega_k^*(\mathbf{X}_{il})\} / \sum_{l=1}^d \exp\{\omega_k^*(\mathbf{X}_{il})\}$, $k = 1, \dots, p$. Let $\boldsymbol{\alpha}^*(\mathbf{X}_{il}, \mathbf{X}_i) = \{\alpha_k^*(\mathbf{X}_{il}, \mathbf{X}_i), k = 1, \dots, p\}$ be a multi-dimensional function, which projects \mathbf{X}_{il} to a p -dimensional space. Let $\mathbf{Z}_i = \{\mathbf{Z}_{il}, l = 1, \dots, d\}^\top$, where \mathbf{Z}_{il} is a p -dimensional auxiliary variable, which can be the signals surrounding the time

segments of interest. Define

$$\mathbf{S}_i(\boldsymbol{\alpha}^*) \equiv \sum_{l=1}^d \{ \mathbf{X}_{il} \boldsymbol{\alpha}^*(\mathbf{X}_{il}, \mathbf{X}_i)^\top + \mathbf{1}_T \boldsymbol{\alpha}^*(\mathbf{X}_{il}, \mathbf{X}_i)^\top \mathbf{Z}_{il} \mathbf{1}_p^\top \}. \quad (1)$$

We assume the conditional density for Y_i given $(\mathbf{X}_i, \mathbf{Z}_i)$, $i = 1, \dots, n$, follows

$$\begin{aligned} f(Y_i | \mathbf{X}_i, \mathbf{Z}_i) &= f[Y_i, g^* \{ \mathbf{S}_i(\boldsymbol{\alpha}^*) \}] \\ &= \exp \left(\frac{Y_i g^* \{ \mathbf{S}_i(\boldsymbol{\alpha}^*) \} - h [g^* \{ \mathbf{S}_i(\boldsymbol{\alpha}^*) \}]}{c(\sigma)} \right), \end{aligned} \quad (2)$$

where h is a known link function, $c(\sigma)$ is a function of scale parameter σ , and $\boldsymbol{\alpha}^*$ and g^* are unknown functions. Since we are interested in $g^* \{ \mathbf{S}_i(\boldsymbol{\alpha}^*) \}$, we will rescale the loss function and assume $c(\sigma) = 1$. With the above model specification, we show that

Proposition 1 *Assume the conditional density function $g^*(\cdot)$ is a continuous differentiable function, $\sum_{l=1}^d \boldsymbol{\alpha}^*(\mathbf{X}_{il}, \mathbf{X}_i) = \mathbf{1}$ for any \mathbf{X}_{il} . Then $\boldsymbol{\alpha}^*(\mathbf{X}_{il}, \mathbf{X}_i)$ and the conditional density function $g^*(\cdot)$ are identifiable.*

The proof of the proposition is presented in Section S3 in the supplementary material.

In this model, $\boldsymbol{\alpha}^*$ represents the weight function, whose value is determined by the input signal patterns, reflecting the significance of a given input channel. Furthermore, by design, $\boldsymbol{\alpha}^*(\mathbf{X}_{il}, \mathbf{X}_i)$ takes into account the signal patterns across all channels, while placing particular emphasis on channel l . Additionally, by allowing $\boldsymbol{\alpha}^*$ to vary with \mathbf{X}_{il} , the number of weights dynamically adjusts according to the channel number, making the resulting weighted combination invariant to the number of channels. Moreover, since only $\mathbf{S}_i(\boldsymbol{\alpha}^*)$ directly influences the outcome, the model is indifferent to the order of the channels. In the model, \mathbf{Z}_i serves as an auxiliary variable to ensure the identifiability of the model. It can be selected as the background signals surrounding \mathbf{X}_i .

3 Deep Learning Estimation

Under the model assumption in (2), we estimate the unknown functions $\boldsymbol{\alpha}^*$ and g^* by minimizing the negative log-likelihood, with a constraint on $\boldsymbol{\alpha}^*$. To flexibly capture the nonlinear structures of $\boldsymbol{\alpha}^*$ and g^* , we propose using deep learning networks to approximate them. More specifically, following the Definition 1, we define the true function space as the following and assume $g^*, \omega_k^* \in \mathcal{G}(q, \mathbf{d}, \mathbf{t}, \boldsymbol{\beta}, K), k = 1, \dots, p$

$$\begin{aligned} \mathcal{G}(q, \mathbf{d}, \mathbf{t}, \boldsymbol{\beta}, K) &\equiv \left\{ f = g_q \circ \dots \circ g_0 : g_u \equiv (g_{uj})_j : [a_u, b_u]^{d_u} \rightarrow [a_{u+1}, b_{u+1}]^{d_{u+1}}, \right. \\ &\quad \left. g_{uj} \in \mathcal{C}_{t_u}^{\beta_u}([a_u, b_u]^{t_u}, K), \text{ for some } |a_i|, |b_i| < K \right\}, \end{aligned}$$

where $\mathbf{d} \equiv (d_0, \dots, d_{q+1})$, $\mathbf{t} \equiv (t_0, \dots, t_q)^\top$, and $\boldsymbol{\beta} \equiv (\beta_0, \dots, \beta_q)^\top$.

Definition 1 *The ball of β -Hölder functions with radius K is defined as*

$$\mathcal{C}_r^\beta(D, K) \equiv \left\{ f : D \subset \mathbb{R}^r \rightarrow \mathbb{R} : \sum_{\boldsymbol{\alpha}: \|\boldsymbol{\alpha}\|_1 < \beta} \|\partial^{\boldsymbol{\alpha}} f\|_\infty + \sum_{\boldsymbol{\alpha}: |\alpha| = \lfloor \beta \rfloor} \sup_{\mathbf{v}_1, \mathbf{v}_2 \in D, \mathbf{v}_1 \neq \mathbf{v}_2} \frac{|\partial^{\boldsymbol{\alpha}} f(\mathbf{v}_1) - \partial^{\boldsymbol{\alpha}} f(\mathbf{v}_2)|}{\|\mathbf{v}_1 - \mathbf{v}_2\|_\infty^{\beta - \lfloor \beta \rfloor}} \leq K \right\},$$

where $\partial^{\boldsymbol{\alpha}} = \partial^{\alpha_1} \dots \partial^{\alpha_r}$ with $\boldsymbol{\alpha} = (\alpha_1, \dots, \alpha_r)^\top \in \mathbb{N}^r$, and $\lfloor \beta \rfloor$ denotes the largest integer strictly smaller than β .

Furthermore, we choose network architectures with L number of layers, and a width vector \mathbf{p}_w , where $\mathbf{p}_w = (p_{w0}, \dots, p_{w(L+1)}) \in \mathbb{N}^{L+1}$, to represent any function in the form of

$$f : \mathbb{R}^{p_{w0}} \rightarrow \mathbb{R}^{p_{w(L+1)}}, \mathbf{x} \rightarrow f(\mathbf{x}) \equiv \mathbf{W}_L \sigma_{\mathbf{v}_L} \mathbf{W}_{L-1} \sigma_{\mathbf{v}_{L-1}}, \dots, \mathbf{W}_1 \sigma_{\mathbf{v}_1} \mathbf{W}_0 \mathbf{x}, \quad (3)$$

where $\sigma_{\mathbf{v}}(y_1, \dots, y_r) = \{\sigma(y_1 - v_1), \dots, \sigma(y_r - v_r)\}$, \mathbf{W}_i is a $p_{w(i+1)} \times p_{wi}$ weight matrix and $\mathbf{v}_i \in \mathbb{R}^{p_{wi}}$ is a shift vector. Define the set of these neural network functions with s number of nonzero parameters as

$$\mathcal{F}(L, \mathbf{p}_w, s, F) \equiv \left\{ f \text{ of the form (3)} : \max_{j=0, \dots, L} \max(\|\mathbf{W}_j\|_\infty, \|\mathbf{v}_j\|_\infty) \leq 1, \right. \\ \left. \sum_{j=1}^L \|\mathbf{W}_j\|_0 + \|\mathbf{v}_j\|_0 \leq s, \sup_{\mathbf{x}} |f(\mathbf{x})| \leq F \right\}.$$

We then obtain the estimator of g^* , α^* as the minimizers of the loss function

$$\mathcal{L}(g, \alpha) = -n^{-1} \sum_{i=1}^n (Y_i g \{S_i(\alpha)\} - h[g \{S_i(\alpha)\}]) \quad \text{subject to} \quad (4)$$

$$g \in \mathcal{F}_g, \omega_k \in \mathcal{F}_{\omega_k}, \alpha_k(\mathbf{x}_l, \mathbf{x}) = \frac{\exp\{\omega_k(\mathbf{x}_l)\}}{\sum_{l=1}^d \exp\{\omega_k(\mathbf{x}_l)\}}, \alpha(\mathbf{x}_l, \mathbf{x}) = \{\alpha_k(\mathbf{x}_l, \mathbf{x}), k = 1, \dots, p\}^\top.$$

Let $\hat{g}, \hat{\alpha} = \{\hat{h}_k, k = 1, \dots, p\}$ be the resulting estimator.

We utilize the deep learning to estimate g^* and α^* . More specifically, we employ the network architecture depicted in Figure 1 to approximate the functions in $\mathcal{G}(q, \mathbf{d}, \mathbf{t}, \beta, K)$. As shown in Figure 1, the core structure consists of a series of recursive CNN layers followed by a fully connected layer. First, we use this block to construct a function that approximates α^* . The resulting function is then fed into another similar block to build a function that approximates g^* .

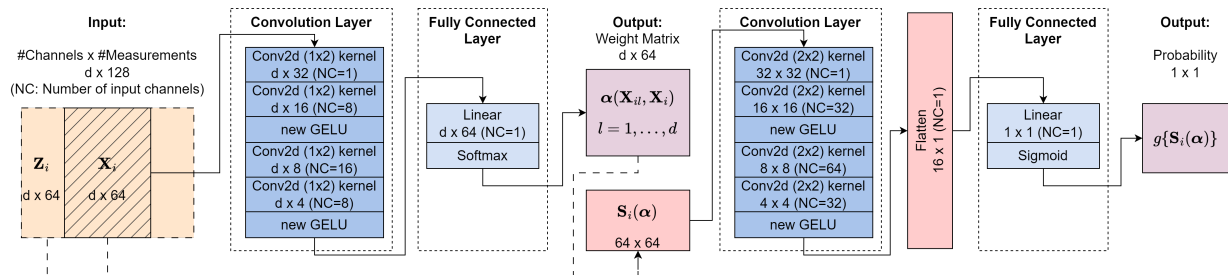


Figure 1: The deep neural networks diagram with two blocks of a series of recursive CNN layers followed by a fully connected layer to approximate unknown functions α^* and g^* in $\mathcal{G}(q, \mathbf{d}, \mathbf{t}, \beta, K)$ of NDL, respectively.

4 Asymptotic Theorem

We show the asymptotic consistency and derive the convergence rate of the deep learning estimators. Below we first present some necessary definitions. Denote $\mathcal{F}_f = \mathcal{F}(L_f, \mathbf{p}_f, s_f, F_f)$

and $\mathcal{G}_f \equiv \mathcal{G}(q_f, \mathbf{d}_f, \mathbf{t}_f, \boldsymbol{\beta}_f, K_f)$, where f can be ω_j, g . Let

$$\phi_{\omega_j n} \equiv \max_{i=0, \dots, q_{\omega_j}} n^{-\frac{2\beta_{\omega_j}^* i}{2\beta_{\omega_j}^* i + t_{\omega_j} i}}, \phi_{gn} \equiv \max_{i=0, \dots, q_g} n^{-\frac{2\beta_g^* i}{2\beta_g^* i + t_g i}},$$

where $\beta_{\omega_j}^* \equiv \beta_{\omega_j} \prod_{l=i+1}^{q_{\omega_j}} \{\min(\beta_{\omega_j l}, 1)\}$ and $\beta_g^* \equiv \beta_g \prod_{l=i+1}^{q_g} \{\min(\beta_{gl}, 1)\}$. Let $g_0, \omega_{0k} \in \mathcal{F}_g, \mathcal{F}_{\omega_k}$, and $\alpha_{0k}(\mathbf{x}_l, \mathbf{x}) = \exp\{\omega_{0k}(\mathbf{x}_l)\} / \sum_{l=1}^d \exp\{\omega_{0k}(\mathbf{x}_l)\}$, such that $g_0 \equiv \operatorname{argmin}_{g \in \mathcal{F}_g} \|g - g^*\|_\infty$, and $\omega_{0k} \equiv \operatorname{argmin}_{\omega_k \in \mathcal{F}_{\omega_k}} \|\omega_k - \omega_k^*\|_\infty$, where g^*, ω_k^* are the true function in $\mathcal{G}_g, \mathcal{G}_{\omega_k}$, respectively. Define

$$\mathcal{H}_k \equiv \left\{ \alpha_k = \exp\{\omega_k(\mathbf{x}_l)\} / \sum_{l=1}^d \exp\{\omega_k(\mathbf{x}_l)\}, \omega_k \in \mathcal{F}_{\omega_k}, k \in 1, \dots, p \right\}.$$

Let $\psi_g = g - g_0$ and $\psi_{\alpha_k} = \alpha_k - \alpha_0$ for arbitrary function $g \in \mathcal{F}_g$ and $\alpha_k \in \mathcal{H}_{\alpha_k}$. Let $\boldsymbol{\psi}_\alpha = \psi_{\alpha_k}, k = 1, \dots, p$. Furthermore, let $\boldsymbol{\alpha}^{(-k)} = (\alpha_1, \dots, \alpha_{k-1}, \alpha_{k+1}, \dots, \alpha_p)$. Let

$$\begin{aligned} & \Omega(g_0, \boldsymbol{\alpha}_0, \psi_g, \boldsymbol{\psi}_\alpha, \boldsymbol{\epsilon}_g^\dagger, \boldsymbol{\epsilon}_\alpha^\dagger) \\ &= \left\{ \frac{\partial^2 \mathcal{L}(g_0 + \epsilon_g \psi_g, \boldsymbol{\alpha})}{\partial \epsilon_g^2} + 2 \sum_{k=1}^p \frac{\partial^2 \mathcal{L}(g_0 + \epsilon_g \psi_g, \alpha_{0k} + \epsilon_{\alpha_k} \psi_{\alpha_k}, \boldsymbol{\alpha}^{(-k)})}{\partial \epsilon_g \partial \epsilon_{\alpha_k}} \right. \\ & \quad \left. + \sum_{k=1}^p \sum_{j=1}^p \frac{\partial^2 \mathcal{L}(g_0, \alpha_{01}, \dots, \alpha_{0l} + \epsilon_{\alpha_l} \psi_{\alpha_l}, \dots, \alpha_{0u} + \epsilon_{\alpha_u} \psi_{\alpha_u}, \dots, \alpha_{0p})}{\partial \epsilon_{\alpha_j} \partial \epsilon_{\alpha_u}} \right\} \Big|_{\epsilon_g = \epsilon_g^\dagger, \epsilon_{\alpha_k} = \epsilon_{\alpha_k}^\dagger, k=1, \dots, p}, \end{aligned}$$

where $\epsilon_g^\dagger, \epsilon_{\alpha_k}^\dagger \in (0, 1), k = 1, \dots, p$ and $\boldsymbol{\epsilon}_\alpha^\dagger = (\epsilon_{\alpha_k}^\dagger, k = 1, \dots, p)^\top$.

Furthermore, we present the following necessary conditions to guarantee the convergence of the estimators.

(C1) Assume $F_{\omega_j} \geq \max(K_{\omega_j}, 1), j = 1, \dots, p$ and $F_g \geq \max(K_g, 1)$.

(C2) Assume $\sum_{i=0}^{q_{\omega_j}} \log_2 \{\max(4t_{\omega_j i}, 4\beta_{\omega_j i})\} \log_2 n \leq L_{\omega_j} \lesssim n\phi_{\omega_j n}, j = 1, \dots, p$,
and $\sum_{i=0}^{q_g} \log_2 \{\max(4t_{gi}, 4\beta_{gi})\} \log_2 n \leq L_g \lesssim n\phi_{gn}$.

(C3) Assume $n\phi_{\omega_j n} \lesssim \min_{u=1, \dots, L} p_{\omega_j u}, j = 1, \dots, p$ and $n\phi_{gn} \lesssim \min_{u=1, \dots, L_g} p_{gu}$.

(C4) Assume $s_{\omega_j} \asymp n\phi_{\omega_j n} \log n, j = 1, \dots, p$ and $s_g \asymp n\phi_{gn} \log n$. And assume $(s_g/L_g)^{L_g/2} \leq M_L < \infty$.

(C5) Assume $X_{ilt}, Z_{ilj} \in [-\max(K_{\omega_j}, K_g, j = 1, \dots, p), \max(K_{\omega_j}, K_g, j = 1, \dots, p)] \subseteq [-C_M, C_M]$.

(C6) Assume $c_\psi < h''(\cdot) < C_\psi$ and $0 < |h'''(\cdot)| < \infty$, and $Y_i - h'[g^* \{\mathbf{S}_i(\boldsymbol{\alpha}^*)\}]$ is a mean zero sub-Gaussian random variable.

(C7) Assume that

$$\begin{aligned} & 0 < \alpha_{\min} E \left[\psi_g \{\mathbf{S}_i(\boldsymbol{\alpha}_0)\}^2 + \sum_{j=1}^p \sum_{l=1}^d T \psi_{\alpha_j}(\mathbf{X}_{il}, \mathbf{X}_i)^2 \right] \\ & \leq \inf_{\epsilon_g, \epsilon_\alpha} E \{ \Omega(g_0, \boldsymbol{\alpha}_0, \psi_g, \boldsymbol{\psi}_\alpha, \epsilon_g, \boldsymbol{\epsilon}_\alpha) \} \leq \sup_{\epsilon_g, \epsilon_\alpha} E \{ \Omega(g_0, \boldsymbol{\alpha}_0, \psi_g, \boldsymbol{\psi}_\alpha, \epsilon_g, \boldsymbol{\epsilon}_\alpha) \} \\ & \leq \alpha_{\max} E \left[\psi_g \{\mathbf{S}_i(\boldsymbol{\alpha}_0)\}^2 + \sum_{j=1}^p \sum_{l=1}^d T \psi_{\alpha_j}(\mathbf{X}_{il}, \mathbf{X}_i)^2 \right] < \infty. \end{aligned}$$

Conditions (C1)–(C4) are standard assumptions that lead to the conclusion that a deep learning network can approximate the true function with an error that vanishes as the sample size increases as shown in Lemma S2 in the supplementary materials. Condition (C5) requires bounded predictors, which are easily met in real data. Condition (C6) and Condition (C7) are commonly assumed for ensuring estimation consistency under the generalized linear model.

Lemma 1 *Assume Conditions (C1)–(C6) hold, and $T, p \leq s_g$, there are positive constants $C_g, C_{\omega_j}, c_g, c_{\omega_j}$ such that with probability one*

$$\begin{aligned} & |h'[g^* \{\mathbf{S}_i(\boldsymbol{\alpha}^*)\}] - h'[g_0 \{\mathbf{S}_i(\boldsymbol{\alpha}_0)\}]| \\ & \leq \left\{ C_g \max_{u=0, \dots, q_g} c_g^{-\frac{\beta_{gu}^*}{t_{gu}}} n^{-\frac{\beta_{gu}^*}{2\beta_{gu}^* + t_{gu}}} + 2C_M M_L \sqrt{d \min(s_g, Tp)} \sup_{j=1, \dots, p} C_{\omega_j} \max_{u=0, \dots, q_{\omega_j}} c_{\omega_j}^{-\frac{\beta_{\omega_j u}^*}{t_{\omega_j u}}} n^{-\frac{\beta_{\omega_j u}^*}{2\beta_{\omega_j u}^* + t_{\omega_j u}}} \right\}. \end{aligned}$$

The proof of the Lemma 1 is presented in Section S4 in the supplementary material. The Lemma shows that the minimal distance between the deep learning approximation of the

regression function and the true regression function depends on how well g_0 and $\boldsymbol{\alpha}_0$ approximate the true values, and this distance decreases at the standard nonparametric rate as the sample size grows.

For the notation convenience, for the positive constants $C_0, A_g, A_{\omega_j}, a_g, a_{\omega_j}, j = 1, \dots, p$, we define

$$\begin{aligned} & \eta(A_g, a_g, \mathbf{A}_\omega, \mathbf{a}_\omega) \\ \equiv & \left\{ A_g \max_{u=0, \dots, q_g} a_g^{-\frac{\beta_{gu}^*}{t_{gu}}} n^{-\frac{\beta_{gu}^*}{2\beta_{gu}^* + t_{gu}}} + 2C_M M_L \sqrt{d \min(s_g, Tp)} \sup_{j=1, \dots, p} A_{\omega_j} \max_{u=0, \dots, q_{\omega_j}} a_{\omega_j}^{-\frac{\beta_{\omega_j u}^*}{t_{\omega_j u}}} n^{-\frac{\beta_{\omega_j u}^*}{2\beta_{\omega_j u}^* + t_{\omega_j u}}} \right\} \\ & + \sqrt{C_0 \log(n)/(cn)} \end{aligned}$$

where $\mathbf{A}_\omega = (A_{\omega_j}, j = 1, \dots, p)^\top$, and $\mathbf{a}_\omega = (a_{\omega_j}, j = 1, \dots, p)^\top$.

Theorem 1 *Let $\psi_{\hat{g}} = \hat{g} - g_0$ and $\psi_{\hat{\alpha}_j} = \hat{\alpha}_j - \alpha_{0j}$. Assume $\hat{\alpha}_j, \alpha_{0j} \in \mathcal{H}_j$, $\omega_j^* \in \mathcal{G}_{\omega_j}$, and $\hat{g}, g_0 \in \mathcal{F}_g$, and $g^* \in \mathcal{G}_g$. Assume $T, p < s_g$. Furthermore assume Condition (C1)–(C7) hold. Let $dP_{\boldsymbol{\alpha}}(\cdot)$ be the probability density function of $\mathbf{S}_i(\boldsymbol{\alpha})$, and assume $\|dP_{\boldsymbol{\alpha}_0}(\mathbf{z})/dP_{\boldsymbol{\alpha}^*}(\mathbf{z})\|_\infty \geq m_h > 0$. Furthermore, let $dP_{\mathbf{X}}(\cdot)$ be the probability density for \mathbf{X}_i . Then there are positive constants $D_g, d_g, \mathbf{D}_\omega = (D_{\omega_j}), \mathbf{d}_\omega = (d_{\omega_j}), D_{g1}, d_{g1}, D_{\omega_j1}, d_{\omega_j1}, c'_H, C_H$ such that*

$$\begin{aligned} & \int \{\hat{g}(\mathbf{z}) - g^*(\mathbf{z})\}^2 dP_{\boldsymbol{\alpha}^*}(\mathbf{z}) + \sum_{j=1}^p \int \sum_{l=1}^d \{\hat{\alpha}_j(\mathbf{x}_l, \mathbf{x}) - \alpha_j^*(\mathbf{x}_l, \mathbf{x})\}^2 dP_{\mathbf{X}}(\mathbf{x}) \\ \leq & \int \{\hat{g}(\mathbf{z}) - g^*(\mathbf{z})\}^2 dP_{\boldsymbol{\alpha}^*}(\mathbf{z}) + T \sum_{j=1}^p \int \sum_{l=1}^d \{\hat{\alpha}_j(\mathbf{x}_l, \mathbf{x}) - \alpha_j^*(\mathbf{x}_l, \mathbf{x})\}^2 dP_{\mathbf{X}}(\mathbf{x}) \\ \leq & 16 \min(m_h, 1)^{-1} \alpha_{\min}^{-1} \left(C_M M_L \eta(D_g, d_g, \mathbf{D}_\omega, \mathbf{d}_\omega) \left[\min(s_g, Tp)^{1/2} \{\log(n)/(cn)\}^{1/4} + \{\log(n)/(cn)\}^{1/4} \right] \right. \\ & \left. + Tp C_1 \log^2(n) \left\{ \phi_{gn} L_g + \sum_{j=1}^p \phi_{\omega_j n} L_{\omega_j} \right\} + C_H Tp/n \right) \\ & + 32 \min(m_h, 1)^{-1} C_M M_L dp \alpha_{\min}^{-2} \eta(D_g, d_g, \mathbf{D}_\omega, \mathbf{d}_\omega)^2 + \left(D_{g1} \phi_{gn} + T \sum_{j=1}^p D_{\omega_j1} \phi_{\omega_j n} \right) \end{aligned}$$

with probability greater than $1 - 6n^{-1} - 2 \exp \left[-nC_1 \log^2(n) \left\{ \phi_{gn} L_g + \sum_{j=1}^p \phi_{\omega_j n} L_{\omega_j} \right\} \right]$.

The proof of the theorem is presented in Section S6 in the supplementary material. To prove the theorem, we demonstrate in Lemma S6 that the first derivative of the objective function has an upper bound that approaches zero as the sample size increases. In Lemma S7, we show that the second derivative is asymptotically a positive definite matrix. We then derive the final results by combining these findings with the convergence of the deep learning function presented in Lemma 1. When T and p are finite, the dominant term in the upper bound is $TpC_1 \log^2(n) \left\{ \phi_{gn}L_g + \sum_{j=1}^p \phi_{\omega_j n}L_{\omega_j} \right\}$, where ϕ_{gn} and $\phi_{\omega_j n}$ are of the order of the inverse of polynomial functions of n . As a result, the upper bound approaches zero as the sample size increases.

5 Real Data Analysis

We apply NDL on three real datasets, including a public scalp EEG dataset from the Temple University Hospital (TUH), an MEG dataset from the University of California, San Francisco (UCSF) and an EEG dataset from the Beijing Tiantan Hospital (BTH).

5.1 Data and preprocessing

TUH data: The TUH dataset is the only publicly available scalp interictal EEG dataset that includes per-channel annotations for EEG data, categorized into six classes (refer to Harati et al. (2015)): (1) spike and sharp wave (SPSW), (2) generalized periodic epileptiform discharges (GPED), (3) periodic lateralized epileptiform discharges (PLED), (4) eye movement (EYEM), (5) artifact (ARTF), and (6) background (BCKG). In these wave-form events (1 second duration), SPSW, GPED and PLED are abnormal events of clinical interests, while EYEM, ARTF and BCKG are normal signals. We show one example in each of the classes in Figure 2. We also summarize the number of segments and patients

in each category in Table 1. The TUH EEG data is collected at a sampling frequency of 250 Hz. We filter the data to retain frequencies between 1 and 45 Hz and divide it into two-second segments. The data is then transformed into the Temporal Central Parasagittal montage, as described in (Lopez et al. 2016), using 22 channels listed in Table S1 in the supplementary material. This montage was chosen because it was used for labeling the data. We train NDL to classify the time segments as either normal or abnormal. Since the TUH dataset provides labels for each channel, in addition to evaluating the accuracy of detecting abnormal samples, we use the dataset to test our hypothesis that NDL can identify key channels by ranking $\hat{\alpha}$.

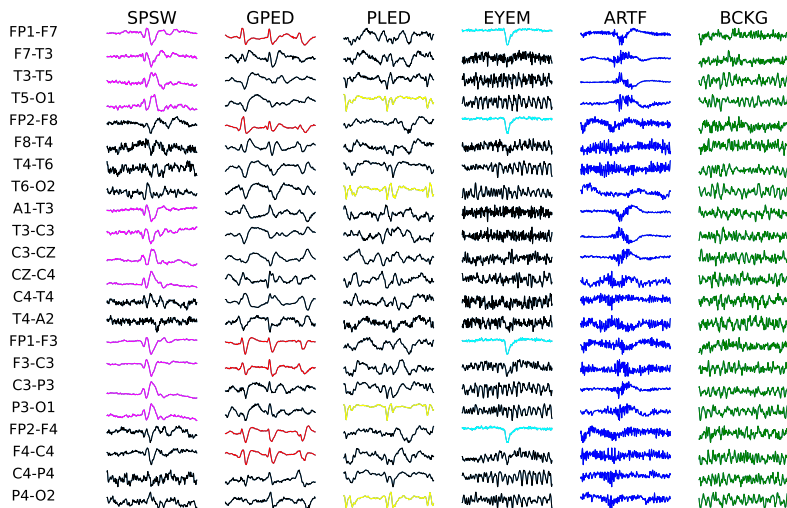


Figure 2: The waveforms of SPSW, GPED, PLED, EYEM, ARTF and BCKG in the TUH data with 22 ACNS TCP montages where highlighted channels are annotated.

MEG data: The MEG data contains 230325 number MEG segments (with 0.25 s duration) separately from 277 epilepsy patients that visited the MEG center at UCSF from 2019 to 2022 who underwent simultaneous EEG and MEG tests. Among these samples,

Table 1: The number of segments containing the six classes of waveform events (SPSW, GPED, PLED, EYEM, ARTF, and BCKG), along with the number of patients who exhibited these waveform events.

	Abnormal			Normal		
	SPSW	GPED	PLED	EYEM	ARTF	BCKG
Training: n segments	139	2404	1890	520	1624	3195
Training: n patients	27	30	29	41	134	200
Testing: n segments	46	819	700	124	519	1187
Testing: n patients	9	21	20	34	41	74

approximately 46% of the segments contain spikes, which are labeled in the clinical notes, while the rest of them are treated as background segments. The MEG data is recorded at a sampling frequency of 600 HZ on 140 channels. We filter the data to retain frequencies between 1 and 45 Hz and divide it into 0.5-second segments. We use 95% randomly selected data as the training data and test the algorithm on the remaining 5% data.

BTH EEG data: We collected a EEG dataset to test the generalizability of NDL across multi-modal data. This dataset consists of 142 EEG segments with 19 channels from 20 patients. Approximately 53 of the segments in these recordings contain spikes, while the rest of them are background signals. This out-of-sample EEG data is recorded at a sampling frequency of 512 HZ. We apply a filter to retain frequencies between 1 and 45 Hz, then segment the data into 0.5-second intervals. The data is then converted to the common average montage. We then test our MEG-trained model on this out-of-sample EEG dataset to evaluate its ability to generalize across different data models.

5.2 Results from TUH data

We apply NDL to the binary classification of normal and abnormal segments in the TUH dataset and report the following metrics evaluated on the testing data.

1. Sensitivity / recall / true positive rate (TPR): $= TP/(TP + FN)$
2. Precision: $= TP/(TP + FP)$
3. Specificity / true negative rate (TNR): $= TN/(TN + FP)$
4. F1 score: $= (2 \times Precision \times Recall)/(Precision + Recall)$
5. PRAUC: The area under the precision-recall curve
6. AUC: The area under the receiver operating characteristic (ROC) curve

where TP , TN , FP and FN represent true positive, true negative, false positive and false negative, respectively. In each time segment, we select the middle half as \mathbf{X} and the remaining portion as \mathbf{Z} . We set p to be equal to the length of the time segment.

We further divide TUH training data into two groups that 80% of the training samples are used for estimating the parameters and 20% of the samples are used for validating the tuning parameter choice. As shown in Figure 3 (a), the train loss and the validation loss decrease rapidly in the first 10 epochs, and become stable after the 40th epoch. In the meanwhile, as shown in Figure 3 (b) the AUC and PRAUC of the validation set stay above and near 90%, respectively, after around 10 epochs. The sensitivity, precision and F1-score all stay above 80% after around 40 epochs with the threshold set to be 0.5.

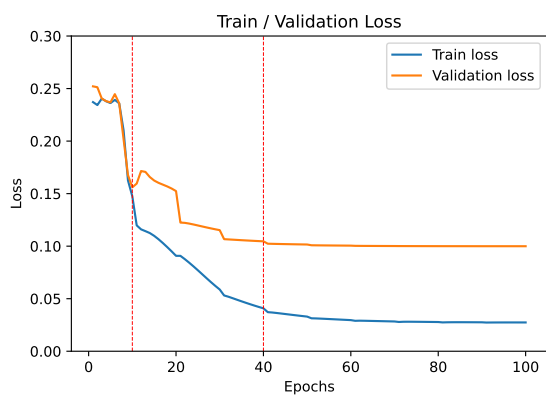
We apply the trained model to the testing data, summarizing the results in Table 2 and presenting the ROC curve and precision-recall curve in Figure 3 (c) and (d). The AUC and PRAUC on the testing data are 93.43% and 92.62%, respectively, demonstrating the

high accuracy and precision of the proposed method. We also compare NDL with the deep learning method proposed in Munia et al. (2023) evaluating on the same datasets. Table 2 presents the testing results of NDL alongside those of the model from Munia et al. (2023). As shown, NDL outperforms the other method in terms of sensitivity, precision, and F1 score. The AUC for the Munia et al. (2023)’s method is not available.

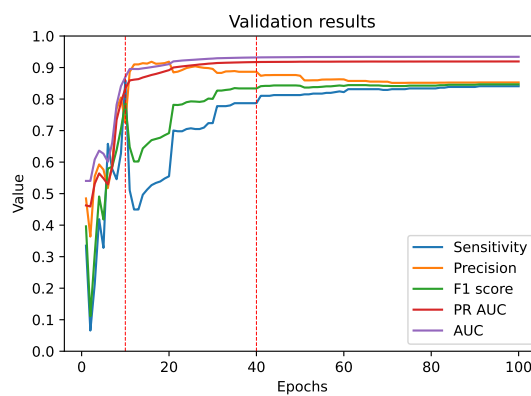
Table 2: A comparison of sensitivity, precision, specificity, F1 score, PRAUC, and AUC between NDL and the results reported in Munia et al. (2023), which are based on the same dataset. Some metrics are not reported in Munia et al. (2023)

TUH	Sen	Prec	Spec	F1 score	PRAUC	AUC
NDL	0.87	0.87	0.88	0.87	0.93	0.93
Munia et al. (2023)	0.75	0.73	-	0.74	-	-

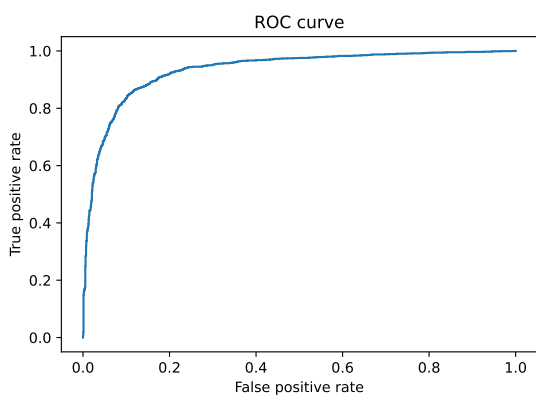
In addition to classifying the EEG time segments as normal or abnormal, we can compute the estimated p -dimensional weight $\hat{\alpha}(\mathbf{X}_{il}, \mathbf{X}_i)$ for each channel l . By summing the p entries of the weight $\hat{\alpha}(\mathbf{X}_{il}, \mathbf{X}_i)$, we determine the importance of channel l as $\mathbf{1}^\top \hat{\alpha}(\mathbf{X}_{il}, \mathbf{X}_i)$. By ranking the channel importances from highest to lowest, we can select the top L channels that are most likely to contain spikes. To assess this approach, we compare the selected top channels with the actual channel labels from the TUH data to determine if our model’s selections outperform random selections. Figure 4 illustrates the probability that the top L segments contain a true spike label, comparing results from the NDL ranking method with those from random selection based on the testing data. We create the 95% confidence interval of the probability through the resample procedures with different initial values or different random seeds. It is clear that NDL offers significantly higher accuracy in identify-



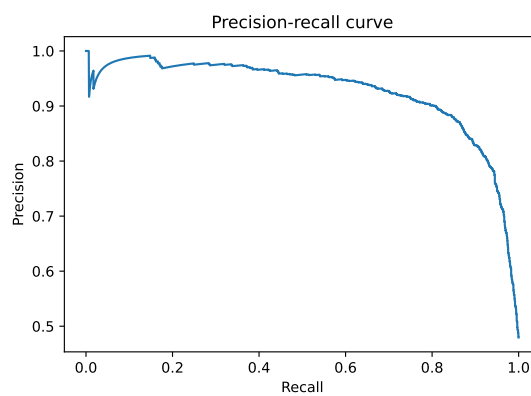
(a) Train loss and validation loss



(b) Validation results



(c) Test ROC curve



(d) Test precision-recall curve

Figure 3: The train loss, validation loss, validation sensitivity, precision, F1 score, PRAUC and AUC with vertical reference lines at the 10th epoch and the 40th epoch, the test ROC curve and precision-recall curve on the TUH data.

ing channels with features that differ from the background. Additionally, it is not surprising that NDL cannot identify background channels because background represent baseline time series without any distinguishable and clinical significant patterns.

5.3 Results from the MEG data

We apply a similar procedure to the MEG dataset, using 95% of the data for training and leaving out 5% for testing. The fitted model achieves an AUC of 91.61% on the testing data. Additional testing results are summarized in Table 3, demonstrating excellent predictive accuracy.

We visualize the distribution of the most important channels using topographical graphs and barplots. The topographical graph is a 2D representation of the value distribution across the brain. Figure 5 contains six topographical graphs from the MEG data, indicating the probabilities of being selected into the top L channel(s) out of 140 MEG sensors on the training set and the testing set. Figure 6 shows the distribution of the top L channels across different brain lobes. Both Figure 5 and Figure 6 indicate that spikes predominantly occur in the temporal lobe. This pattern is observed in both the left and right hemispheres. This is consistent with common clinical finding that the temporal lobes are the areas of the brain that most commonly give rise to seizures (McIntosh et al. 2019).

Table 3: The test results of sensitivity, precision, specificity, F1 score, PRAUC and AUC in percentage (%) from the MEG dataset.

	Sen(%)	Prec(%)	Spec(%)	F1(%)	PRAUC(%)	AUC(%)
MEG dataset	77.07	84.26	91.39	80.50	87.20	91.61

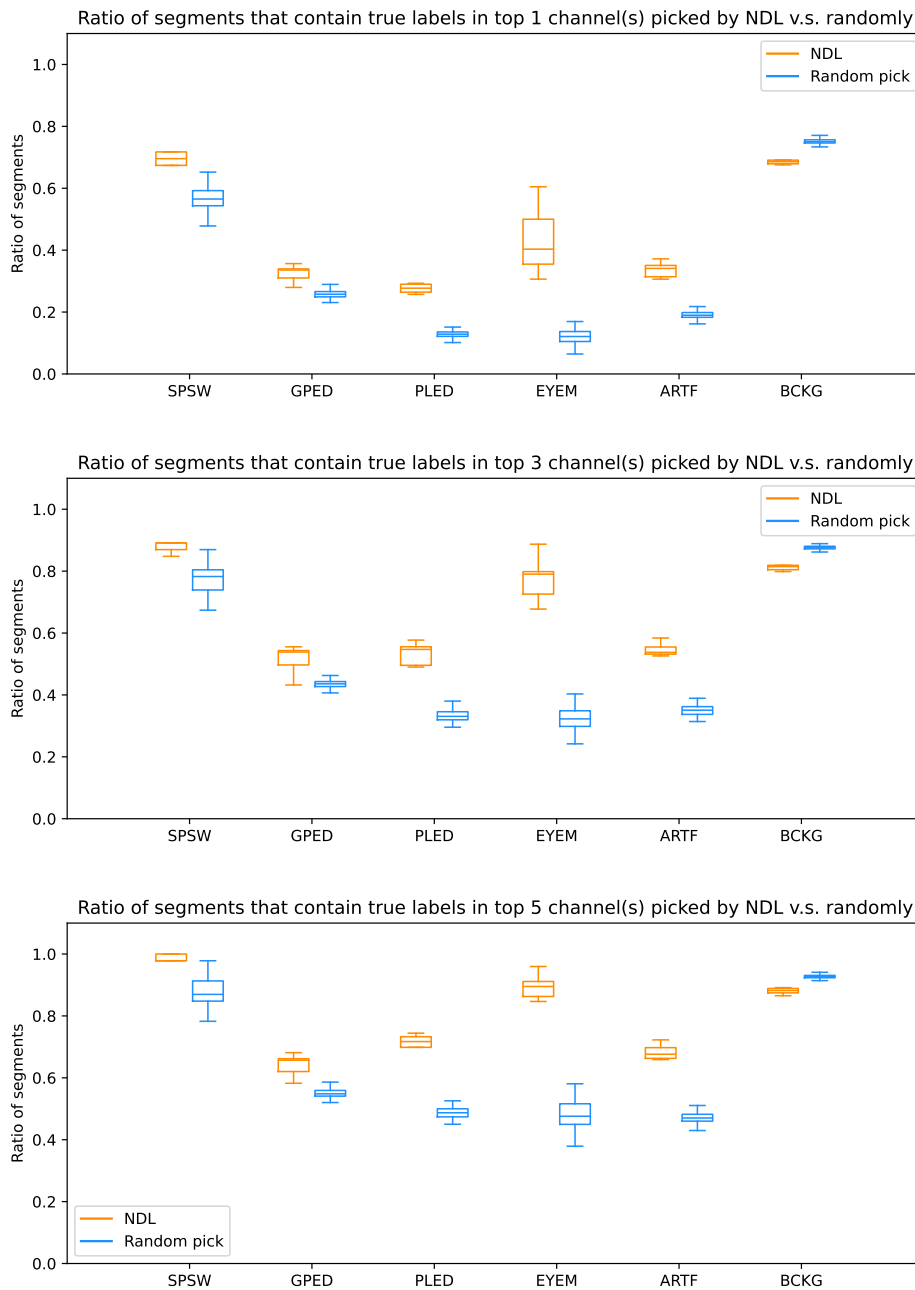


Figure 4: Side-by-side boxplots of the ratio of segments, that contain true labels in any of the top L channels, $L = 1, 3, 5$, selected by NDL with different initial values versus 100 times of random picks, from the TUH data.

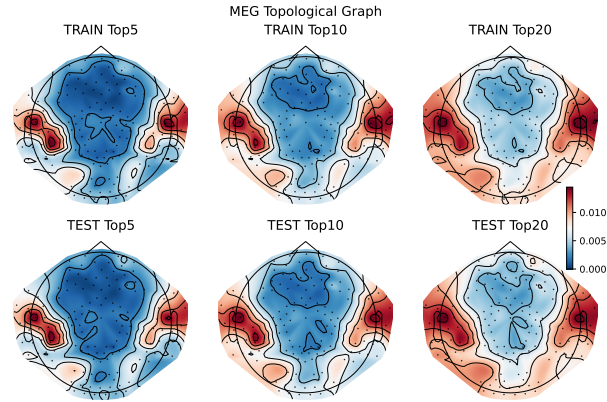


Figure 5: The MEG topological graphs illustrating the probabilities of being selected into the top L channels, where $L = 5, 10, 20$, out of 140 MEG sensors for both the training and the testing set of the MEG dataset.

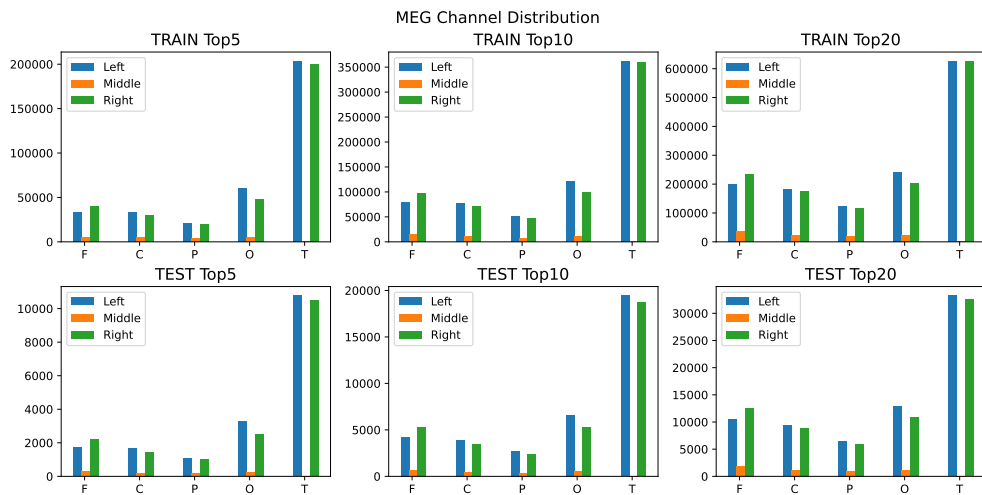


Figure 6: The bar plots of the distributions of top L channels, $L = 5, 10, 20$, out of 140 MEG sensors among 5 lobes, including the frontal, center, parietal, occipital and temporal lobes, by the left, right hemispheres and the midline of the brain for both the training set and the testing set of the MEG dataset.

5.4 Results from the BTH EEG data

We also evaluate the model on the BTH EEG dataset. The model, trained on the MEG dataset, is tested to assess its generalizability across different modalities with varying channels. On the BTH EEG dataset, the model achieves an AUC of 84.18% and a sensitivity of 94.34%, demonstrating that the NDL model trained on MEG data can perform effectively on detecting EEG spikes.

We present three topographical graphs in Figure 7 showing the probability of being selected among the top L channels. Figure 8 shows the distribution of top L channels in different lobes. Interestingly, in addition to the temporal lobes, the pre-frontal regions are also frequently selected. This is not unexpected, as scalp EEG spikes can often be confused with eye movements. More data are needed to fine-tune the model for better adaptation to EEG data. It is worth mentioning that we also apply the model trained on the TUH data on the BTH EEG data. However, the labeled time segments that contain spikes in the TUH dataset are one second wide, which is too broad for accurately capturing spikes. As a result, the model does not perform well on the BTH EEG data, and we have opted not to show those results here.

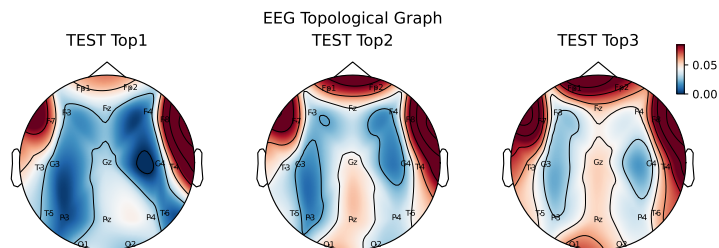


Figure 7: The EEG topological graphs illustrating the probabilities of being selected into the top L channels, $L = 1, 2, 3$, out of 19 EEG sensors tested on the BTH EEG dataset.

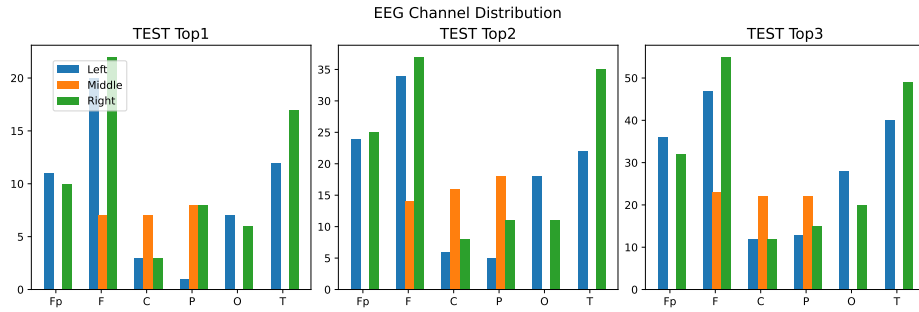


Figure 8: The bar plots of the distributions of top L channels, $L = 1, 2, 3$, out of 19 EEG sensors among 5 lobes, including the frontal, center, parietal, occipital and temporal lobes, by the left, right hemispheres and the midline of the brain for both the training set and the testing set of the BTH EEG dataset.

5.5 Procedures to adopt to continuous time series data

The neurophysiology data are recorded continuously over time in real-world settings, rather than being segmented as they were in our model development. Therefore, we introduce an algorithm to apply NDL to continuous time series data in real settings. In Algorithm 1, we use a sliding window technique to assess the probability of each overlapping window containing a spike. We then identify time segments where this probability exceeds a specified threshold C as our candidates. Lastly, a non-maximum suppression algorithm is employed to remove overlapping candidates, yielding the final set of identified segments.

Algorithm 1 The sliding window algorithm

Input: Preprocessed MEG and EEG recordings with d sensors and a total of T_0 time points; a segmentation length T ; a cutoff C .

for $t = T/2, \dots, T_0 - T/2$ **do**

Set the window between the $(t - T/2 + 1)^{th}$ and the $(t + T/2)^{th}$ time point.

Estimate the probability $\hat{g}_{(t)}$ and the channel weight $\hat{\alpha}_{l,(t)}, l = 1, \dots, d$.

if $\hat{g}_{(t)} > C$ and $\mathbf{1}^\top \hat{\alpha}_{l,(t)} > (1.5/d)(\sum_{l=1}^d \mathbf{1}^\top \hat{\alpha}_{l,(t)})$ **then**

Select the segment at the time point t as a candidate segment that contains a spike.

end if

Remove duplicate annotations by first clustering the candidate segments based on their time. Then, select the segment with the highest spike probability within each cluster as the final spike representation. This process utilizes the Density-Based Spatial Clustering of Applications with Noise (DBSCAN) method (Ester et al. 1996) for clustering.

end for

We implement Algorithm 1 on the MEG testing data and the BTH EEG data and select some detection examples shown in Figure 9. Figure 9 (a) shows an example of MEG test data. The first detection successfully identified true spikes in the right temporal lobe, followed by an additional detection shortly after. Although the later detection occurred outside the 0.25s window of the labeled time, it is still valid because the manual label marks the onset of the spike, and spikes can propagate to other channels. Additionally, our detection results clearly capture the true channels containing spikes. Figure 9 (b) presents an example of EEG results from the BTH dataset. The first detection successfully

identifies a true spike on the F7-avg channel, while the second and third detections capture eye movements appearing on the Fp1-avg and Fp2-avg channels. Since eye movement artifacts typically manifest simultaneously on the Fp1-avg and Fp2-avg channels, which are closest to the eyes, the detection of these top channels helps in eliminating false positive annotations.

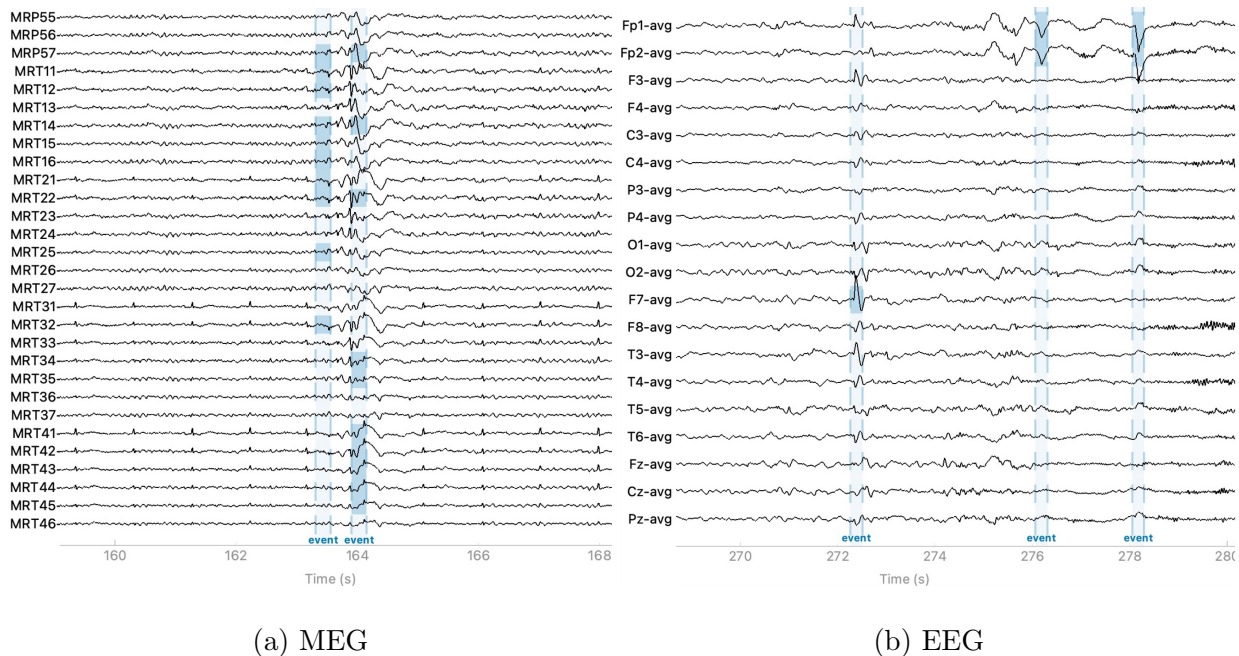


Figure 9: MEG and EEG recordings annotated by NDL using Algorithm 1, with blue segments demonstrating spike annotations by NDL, in which the highlighted channels are top channels whose weights exceed 1.5 times of the mean weight selected by NDL.

6 Simluation

We evaluate NDL using simulation studies with different sample sizes n to examine the convergence of the estimation procedure. We generate \mathbf{X}_i and \mathbf{Z}_i through the TUH EEG data by the following procedures:

1. Randomly select $d \times (T + p)$ signal sub-matrices from TUH EEG data.

2. Standardize each sub-matrix by subtracting the row mean and dividing by the standard deviation of the matrix elements.
3. Select the $\frac{p}{2} + 1^{th}, \dots, \frac{p}{2} + T^{th}$ columns of the sub-matrix as \mathbf{X}_i .
4. Combine the rest columns of the sub-matrix as \mathbf{Z}_i .

where \mathbf{X}_i is a $d \times T$ matrix and \mathbf{Z}_i is a $d \times p$ matrix. In the simulation, we set $d = 22$, $T = 64$ and $p = 64$.

We choose $\omega_k^*(\mathbf{X}_{il}), k = 1, \dots, p$ randomly with replacement from the set

$$\left\{ \ln \left(\sum_{t=1}^T (X_{ilt})^2 / T - \mu_{il}^2 \right), -\ln \left(\sum_{t=1}^T (X_{ilt})^2 / T - \mu_{il}^2 \right), \right. \\ \left. \left(\sum_{t=1}^T (z_{ilt})^3 / T \right), - \left(\sum_{t=1}^T (z_{ilt})^3 / T \right), \left(\sum_{t=1}^T (z_{ilt})^4 / T - 3 \right), - \left(\sum_{t=1}^T (z_{ilt})^4 / T - 3 \right), \right. \\ \left. \ln \left(\sum_{t=1}^T |X_{ilt} \sin(X_{ilt})| \right), \ln \left(\sum_{t=1}^T |X_{ilt} \cos(X_{ilt})| \right) \right\}$$

where $z_{ilt} = (X_{ilt} - \mu_{il}) / \sigma_{il}$ with $\mu_{il} = \sum_{t=1}^T X_{ilt} / T$ and $\sigma_{il} = \sqrt{\sum_{t=1}^T (X_{ilt})^2 / T - \mu_{il}^2}$.

We obtain $\boldsymbol{\alpha}^*(\mathbf{X}_{il}, \mathbf{X}_i)$ through $\alpha_k^*(\mathbf{X}_{il}, \mathbf{X}_i) = \exp\{\omega_k^*(\mathbf{X}_{il})\} / \sum_{l=1}^d \exp\{\omega_l^*(\mathbf{X}_{il})\}$, $k = 1, \dots, p$. Furthermore, we generate $\boldsymbol{\beta}_1 = (\beta_{11}, \dots, \beta_{1T})^\top$ and $\boldsymbol{\beta}_2 = (\beta_{21}, \dots, \beta_{2p})^\top$ from standard multivariate normal distributions and generate β_0 from a standard normal distribution fixed across simulations. Then we define the probability of success as

$$g^* \{ \mathbf{S}_i(\boldsymbol{\alpha}^*) \} = \frac{1}{e^{-(\boldsymbol{\beta}_1^\top \mathbf{S}_i(\boldsymbol{\alpha}^*) \boldsymbol{\beta}_2 + \beta_0)} + 1}$$

Finally, we sample Y_i as a Bernoulli variable with the probability of success to be $g^* \{ \mathbf{S}_i(\boldsymbol{\alpha}^*) \}$.

We measure the distance between the true function and the estimators by the mean absolute errors (MAE) for each sample set $\{(\mathbf{X}_i, \mathbf{Z}_i, Y_i), i = 1, \dots, n\}$

$$\text{MAE}(\boldsymbol{\alpha}^*) = \frac{1}{n} \sum_{i=1}^n \left\| \{ \boldsymbol{\alpha}^*(\mathbf{X}_{il}, \mathbf{X}_i), l = 1, \dots, d \}^\top - \{ \hat{\boldsymbol{\alpha}}(\mathbf{X}_{il}, \mathbf{X}_i), l = 1, \dots, d \}^\top \right\|_2$$

and the

$$\text{MAE}(g^*) = \frac{1}{n} \sum_{i=1}^n |g^* \{ \mathbf{S}_i(\hat{\boldsymbol{\alpha}}) \} - \hat{g} \{ \mathbf{S}_i(\hat{\boldsymbol{\alpha}}) \}|$$

where n is the sample size.

We generate datasets from five settings with varying sample size $n_j = 2^{10+j}$, $j = 1, \dots, 5$. The simulation is repeated 10 times. Figure 10 demonstrates that both $\text{MAE}(\boldsymbol{\alpha}^*)$ and $\text{MAE}(g^*)$ reduce as the sample size n increases. This shows that $\boldsymbol{\alpha}^*(\mathbf{X}_{il}, \mathbf{X}_i)$ and $g^* \{S_i(\boldsymbol{\alpha}^*)\}$ are identifiable and our estimators converge to the true values when the sample size increases.

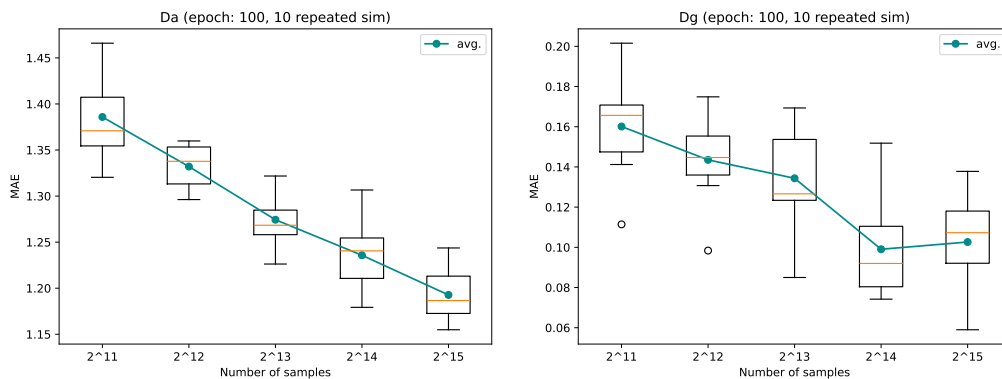


Figure 10: The boxplots and the averages of $\text{MAE}(\boldsymbol{\alpha}^*)$ and $\text{MAE}(g^*)$ at the 100th epoch with 10 repeated simulations using from 2048 to 32768 samples.

7 Conclusion and Discussion

We have developed the NDL method as an interpretable alternative to traditional deep learning for solving the spike detection problem. This method can adapt to different channel types, making it a foundational model for neurophysiological data analysis. We have established the model’s identifiability and demonstrated the asymptotic consistency of its estimation procedures. NDL has been applied to publicly available TUH EEG data, private MEG data from UCSF, and EEG data from BTH. Our analysis shows that NDL outperforms existing methods in terms of sensitivity and specificity in spike detection. Moreover,

it effectively identifies significant channels containing relevant events. Additionally, we demonstrate that a model trained on MEG data can be successfully applied to EEG data, highlighting NDL’s capacity to integrate multiple datasets and serve as a foundation model that can be fine-tuned for different targets.

In this paper, our model is trained on TUH data from 370 subjects and MEG data from 277 subjects. Due to the limited sample sizes, the model may not fully capture the variation in spike waveforms across different populations. We are currently collaborating with clinicians to label additional EEG and MEG data to improve the model’s accuracy across a broader range of populations. The tools developed in this paper will be used as a screening process to identify spike candidates, streamlining the labeling process in this larger study.

False discovery has long been a challenge in spike detection, and we acknowledge that our model trained on the limited samples does not fully address this issue. However, identifying key channels can help reduce false discoveries. For instance, if the first two detected channels are those nearest to the eyes, the spike is more likely related to eye movements. Additionally, training the model on larger datasets, which we are currently preparing, could significantly lower the false discovery rate.

References

- Antoniades, A., Spyrou, L., Took, C. C. & Sanei, S. (2016), Deep learning for epileptic intracranial eeg data, *in* ‘2016 IEEE 26th International Workshop on Machine Learning for Signal Processing (MLSP)’, IEEE, pp. 1–6.
- Baud, M. O., Kleen, J. K., Anumanchipalli, G. K., Hamilton, L. S., Tan, Y.-L., Knowlton, R. & Chang, E. F. (2018), ‘Unsupervised learning of spatiotemporal interictal discharges in focal epilepsy’, *Neurosurgery* **83**(4), 683–691.
- Chung, Y. G., Lee, W.-J., Na, S. M., Kim, H., Hwang, H., Yun, C.-H. & Kim, K. J. (2023), ‘Deep learning-based automated detection and multiclass classification of focal interictal epileptiform discharges in scalp electroencephalograms’, *Scientific Reports* **13**(1), 6755.
- Clarke, S., Karoly, P. J., Nurse, E., Seneviratne, U., Taylor, J., Knight-Sadler, R., Kerr, R., Moore, B., Hennessy, P., Mendis, D. et al. (2021), ‘Computer-assisted eeg diagnostic review for idiopathic generalized epilepsy’, *Epilepsy & Behavior* **121**, 106556.
- Ester, M., Kriegel, H.-P., Sander, J., Xu, X. et al. (1996), A density-based algorithm for discovering clusters in large spatial databases with noise, *in* ‘kdd’, Vol. 96, pp. 226–231.
- Fukumori, K., Yoshida, N., Sugano, H., Nakajima, M. & Tanaka, T. (2021), ‘Epileptic spike detection using neural networks with linear-phase convolutions’, *IEEE Journal of Biomedical and Health Informatics* **26**(3), 1045–1056.
- Goelz, H., Jones, R. D. & Bones, P. J. (2000), ‘Wavelet analysis of transient biomedical signals and its application to detection of epileptiform activity in the eeg’, *Clinical electroencephalography* **31**(4), 181–191.

- Golmohammadi, M., Harati Nejad Torbati, A. H., Lopez de Diego, S., Obeid, I. & Picone, J. (2019), ‘Automatic analysis of eegs using big data and hybrid deep learning architectures’, *Frontiers in human neuroscience* **13**, 76.
- Harati, A., Golmohammadi, M., Lopez, S., Obeid, I. & Picone, J. (2015), Improved eeg event classification using differential energy, *in* ‘2015 IEEE Signal Processing in Medicine and Biology Symposium (SPMB)’, IEEE, pp. 1–4.
- Jing, J., Sun, H., Kim, J. A., Herlopian, A., Karakis, I., Ng, M., Halford, J. J., Maus, D., Chan, F., Dolatshahi, M. et al. (2020), ‘Development of expert-level automated detection of epileptiform discharges during electroencephalogram interpretation’, *JAMA neurology* **77**(1), 103–108.
- Johansen, A. R., Jin, J., Maszczyk, T., Dauwels, J., Cash, S. S. & Westover, M. B. (2016), Epileptiform spike detection via convolutional neural networks, *in* ‘2016 IEEE International Conference on Acoustics, Speech and Signal Processing (ICASSP)’, IEEE, pp. 754–758.
- Lopez, S., Gross, A., Yang, S., Golmohammadi, M., Obeid, I. & Picone, J. (2016), An analysis of two common reference points for eegs, *in* ‘2016 IEEE signal processing in medicine and biology symposium (SPMB)’, IEEE, pp. 1–5.
- McIntosh, W. C. et al. (2019), ‘Temporal seizure’.
- Medvedev, A., Agoureeva, G. & Murro, A. (2019), ‘A long short-term memory neural network for the detection of epileptiform spikes and high frequency oscillations’, *Scientific reports* **9**(1), 19374.
- Munia, M. S., Nourani, M., Harvey, J. & Dave, H. (2023), Interictal epileptiform discharge

detection using multi-head deep convolutional neural network, *in* ‘2023 45th Annual International Conference of the IEEE Engineering in Medicine & Biology Society (EMBC)’, IEEE, pp. 1–4.

Schmidt-Hieber, J. (2020), ‘Nonparametric regression using deep neural networks with ReLU activation function’, *The Annals of Statistics* **48**(4), 1875 – 1897.

URL: <https://doi.org/10.1214/19-AOS1875>

Smith, E. H., Liou, J.-y., Merricks, E. M., Davis, T., Thomson, K., Greger, B., House, P., Emerson, R. G., Goodman, R., McKhann, G. M. et al. (2022), ‘Human interictal epileptiform discharges are bidirectional traveling waves echoing ictal discharges’, *Life* **11**, e73541.

Thomas, J., Jin, J., Thangavel, P., Bagheri, E., Yuvaraj, R., Dauwels, J., Rathakrishnan, R., Halford, J. J., Cash, S. S. & Westover, B. (2020), ‘Automated detection of interictal epileptiform discharges from scalp electroencephalograms by convolutional neural networks’, *International journal of neural systems* **30**(11), 2050030.

Tjepkema-Cloostermans, M. C., de Carvalho, R. C. & van Putten, M. J. (2018), ‘Deep learning for detection of focal epileptiform discharges from scalp eeg recordings’, *Clinical neurophysiology* **129**(10), 2191–2196.

Torres, R. E. & Butter, I. H. (1996), ‘The impact of eeg technology on health manpower’, *American Journal of Electroneurodiagnostic Technology* **36**(2), 114–132.

Vershynin, R. (2010), ‘Introduction to the non-asymptotic analysis of random matrices’, *arXiv preprint arXiv:1011.3027*.

Wilson, S. B., Turner, C. A., Emerson, R. G. & Scheuer, M. L. (1999), ‘Spike detec-

tion ii: automatic, perception-based detection and clustering', *Clinical neurophysiology* **110**(3), 404-411.

World Health Organization (2024), 'Epilepsy', <https://www.who.int/news-room/fact-sheets/detail/epilepsy>. Accessed: 2024-02-07.

Supplementary Materials for “Nested Deep Learning Model Towards a Foundation Model for Brain Signal Data.”

S1 Additional Notations

We write $a \lesssim b$ if there exists a constant C such that $a \leq Cb$ for all n . Moreover, $a \asymp b$ means that $a \lesssim b$ and $b \lesssim a$. Let $\mathcal{N}(\delta, \mathcal{F}, \|\cdot\|_\infty)$ be the covering number, that is, the minimal number of $\|\cdot\|_\infty$ -balls with radius δ that covers \mathcal{F} . For a variable X , we define $\|X\|_{\psi_2} = \sup_{k \geq 1} k^{-1/2} (E|X|^k)^{1/k}$ and define $\|X\|_{\psi_1} = \sup_{k \geq 1} k^{-1} (E|X|^k)^{1/k}$.

S2 Useful lemmas

Lemma S1 *Let \mathcal{F} be a sub-field of the sigma-field generated by X . Let $K_j(\mathcal{F}) > 0, j = 1, \dots, 4$ be functions of random variables in \mathcal{F} . Then, the following properties 1, 2, and 3 are equivalent, and when $E(X|\mathcal{F}) = 0$, they are further equivalent to property 4. In addition, $K_j(\mathcal{F})$ can be chosen to satisfy $0 < c < K_j(\mathcal{F})/K_k(\mathcal{F}) < C < \infty$, for all $k, j \in \{1, 2, 3, 4\}$, where c, C are absolute constants.*

1. *Tail: There exists $K_1(\mathcal{F})$ such that $\Pr(|X| > t|\mathcal{F}) \leq \exp\{1 - t^2/K_1^2(\mathcal{F})\}$;*
2. *Moments: There exists $K_2(\mathcal{F})$ such that $E(|X|^k|\mathcal{F})^{1/k} \leq K_2(\mathcal{F})\sqrt{k}$, for all $k \geq 1$;*
3. *Super-exponential moment: There exists $K_3(\mathcal{F})$ such that $E[\exp\{X^2/K_3^2(\mathcal{F})\}|\mathcal{F}] \leq e$;*
4. *Let $E(X|\mathcal{F}) = 0$. There exists $K_4(\mathcal{F})$ such that $E\{\exp(tX)|\mathcal{F}\} \leq \exp\{t^2 K_4^2(\mathcal{F})\}$.*

Definition 2 *A random variable X that satisfies one of the equivalent properties in Lemma S1 is named a conditional sub-Gaussian random variable with respect to the sub-sigma field \mathcal{F} . The conditional sub-gaussian norm of X with respect to \mathcal{F} , denoted by $\|X\|_{\psi_2(\mathcal{F})}$, is defined as the smallest $K_2(\mathcal{F})$ in property 2. That is,*

$$\|X\|_{\psi_2(\mathcal{F})} = \sup_{k \geq 1} k^{-1/2} E(|X|^k|\mathcal{F})^{1/k}.$$

Lemma S2 *Assume $f \in \mathcal{G}(q, \mathbf{d}, \mathbf{t}, \boldsymbol{\beta}, K)$. Furthermore, let $\beta_i^* \equiv \beta_i \prod_{l=i+1}^q \{\min(\beta_l, 1)\}$ and $\phi_n \equiv \max_{i=0, \dots, q} n^{-2\beta_i^*/(2\beta_i^* + t_i)}$. Define a function space $\mathcal{F}(L, (p_{wu})_{u=0, \dots, L+1}, s, F)$ satisfying the following conditions:*

- (i) $F \geq \max(K, 1)$,
- (ii) $\sum_{i=0}^q \log_2 \{\max(4t_i, 4\beta_i)\} \log_2 n \leq L \lesssim n\phi_n$,
- (iii) $n\phi_n \lesssim \min_{u=1, \dots, L} p_{wu}$,
- (iv) $s \asymp n\phi_n \log n$.

Then there exists a $f_0 \in \mathcal{F}(L, (p_{wu})_{u=0, \dots, L+1}, s, F)$ such that

$$\|f_0 - f\|_\infty^2 \leq C \max_{v=0, \dots, q} c^{-\frac{2\beta_v^*}{t_v}} n^{-\frac{2\beta_v^*}{2\beta_v^* + t_v}}.$$

where C, c are constants only depends on $q, \mathbf{d}, \mathbf{t}, \boldsymbol{\beta}$.

Proof: This lemma is a direct consequence of (26) in Schmidt-Hieber (2020).

Lemma S3 For any $\delta > 0$, we have

$$\log \mathcal{N} \{ \delta, \mathcal{F}(L, \mathbf{p}_w, s, \infty), \|\cdot\|_\infty \} \leq (s+1) \log \{ 2^{2L+5} \delta^{-1} (L+1) p_{w0}^2 p_{wL+1}^2 s^{2L} \}.$$

Proof: This lemma is a direct consequence of Lemma 4 in Schmidt-Hieber (2020).

Lemma S4 Let X_1, \dots, X_N be independent centered sub-Gaussian random variable, and let $K = \max_i \|X_i\|_{\psi_2}$. Then for every $\mathbf{a} = (a_1, \dots, a_N)^\top \in \mathbb{R}^N$ and every $t \geq 0$, we have

$$\Pr \left(\left| \sum_{i=1}^N a_i X_i \right| \right) \leq e \exp \left(-\frac{ct^2}{K^2 \|\mathbf{a}\|_2^2} \right),$$

where $c > 0$ is an absolute constant.

Proof: This is a direct consequence of Proposition 5.10 in Vershynin (2010).

Lemma S5 . Let X_1, \dots, X_N be independent centered sub-exponential random variables, and $K = \max_i \|X_i\|_{\psi_1}$. Then for every $\mathbf{a} = (a_1, \dots, a_N)^\top \in \mathbb{R}^N$ and every $t > 0$, we have

$$\Pr \left(\left| \sum_{i=1}^N a_i X_i \right| \right) \leq 2 \exp \left\{ -c \min \left(\frac{t^2}{K^2 \|\mathbf{a}\|_2^2}, \frac{t}{K \|\mathbf{a}\|_\infty} \right) \right\},$$

where $c > 0$ is an absolute constant.

S3 Proof of Proposition 1

Proof: For notation simplicity, we omit index i in the following proofs. If $\boldsymbol{\alpha}(\mathbf{X}_t, \mathbf{X})$ and the conditional density function $g\{\mathbf{S}(\boldsymbol{\alpha})\}$ are not identifiable, then we will have $\tilde{g}, \tilde{\boldsymbol{\alpha}}$ such

that $(g, \boldsymbol{\alpha}) \neq (\tilde{g}, \tilde{\boldsymbol{\alpha}})$, but

$$\begin{aligned} & g \left\{ \sum_{l=1}^d \mathbf{X}_l \boldsymbol{\alpha}(\mathbf{X}_l, \mathbf{X})^\top + \mathbf{1}_T \boldsymbol{\alpha}(\mathbf{X}_l, \mathbf{X})^\top \mathbf{Z}_l \mathbf{1}_p^\top \right\} \\ &= \tilde{g} \left\{ \sum_{l=1}^d \mathbf{X}_l \tilde{\boldsymbol{\alpha}}(\mathbf{X}_l, \mathbf{X})^\top + \mathbf{1}_T \tilde{\boldsymbol{\alpha}}(\mathbf{X}_l, \mathbf{X})^\top \mathbf{Z}_l \mathbf{1}_p^\top \right\} \end{aligned} \quad (\text{S1})$$

for any given $\mathbf{X}_l, \mathbf{Z}_l$. Now replacing \mathbf{Z}_l by $\mathbf{Z}_l + \xi I(\mathbf{X}_l = \mathbf{X}_u) \mathbf{e}_j$ in (S1) where \mathbf{e}_j is a length p unit vector with the j th element 1, and $I(\cdot)$ is an indicator function, Taking the derivative of both sides with respect to ξ and evaluate at $\xi = 0$, denote \mathbf{M}_{qt} be the q, t th entry of matrix, \mathbf{M} , then the left hand side follows

$$\begin{aligned} & \frac{\partial f \left\{ \sum_{l=1}^d \mathbf{X}_l \boldsymbol{\alpha}(\mathbf{X}_l, \mathbf{X})^\top + \mathbf{1}_T \boldsymbol{\alpha}(\mathbf{X}_l, \mathbf{X})^\top \{ \mathbf{Z}_l + \xi I(\mathbf{X}_l = \mathbf{X}_u) \mathbf{e}_j \} \mathbf{1}_p^\top \right\}}{\partial \xi} \Big|_{\xi=0} \\ &= \sum_{q=1}^p \sum_{t=1}^T \frac{\partial g \left\{ \sum_{l=1}^d \mathbf{X}_l \boldsymbol{\alpha}(\mathbf{X}_l, \mathbf{X})^\top + \mathbf{1}_T \boldsymbol{\alpha}(\mathbf{X}_l, \mathbf{X})^\top \mathbf{Z}_l \mathbf{1}_p^\top \right\}}{\partial \left\{ \sum_{l=1}^d \mathbf{X}_l \boldsymbol{\alpha}(\mathbf{X}_l, \mathbf{X})^\top + \mathbf{1}_T \boldsymbol{\alpha}(\mathbf{X}_l, \mathbf{X})^\top \mathbf{Z}_l \mathbf{1}_p^\top \right\}_{qt}} \sum_{l=1}^d \boldsymbol{\alpha}(\mathbf{X}_l, \mathbf{X})^\top \mathbf{e}_j I(\mathbf{X}_l = \mathbf{X}_u) \\ &= \sum_{q=1}^p \sum_{t=1}^T \frac{\partial g \left\{ \sum_{l=1}^d \mathbf{X}_l \boldsymbol{\alpha}(\mathbf{X}_l, \mathbf{X})^\top + \mathbf{1}_T \boldsymbol{\alpha}(\mathbf{X}_l, \mathbf{X})^\top \mathbf{Z}_l \mathbf{1}_p^\top \right\}}{\partial \left\{ \sum_{l=1}^d \mathbf{X}_l \boldsymbol{\alpha}(\mathbf{X}_l, \mathbf{X})^\top + \mathbf{1}_T \boldsymbol{\alpha}(\mathbf{X}_l, \mathbf{X})^\top \mathbf{Z}_l \mathbf{1}_p^\top \right\}_{qt}} \alpha_j(\mathbf{X}_u, \mathbf{X}). \end{aligned}$$

The same follows for the right hand side, and hence we have

$$\sum_{q=1}^p \sum_{t=1}^T \frac{\partial g\{\mathbf{S}(\boldsymbol{\alpha})\}}{\partial S_{qt}(\boldsymbol{\alpha})} \alpha_j(\mathbf{X}_u, \mathbf{X}) = \sum_{q=1}^p \sum_{t=1}^T \frac{\partial \tilde{g}\{\mathbf{S}(\tilde{\boldsymbol{\alpha}})\}}{\partial S_{qt}(\tilde{\boldsymbol{\alpha}})} \tilde{\alpha}_j(\mathbf{X}_u, \mathbf{X}).$$

Now summing across \mathbf{u} , noting that $\partial g\{\mathbf{S}(\boldsymbol{\alpha})\}/\partial S_{qt}(\boldsymbol{\alpha}), \partial \tilde{g}\{\mathbf{S}(\tilde{\boldsymbol{\alpha}})\}/\partial S_{qt}(\tilde{\boldsymbol{\alpha}})$ do not contain \mathbf{X}_u , and $\sum_{u=1}^d \alpha_j(\mathbf{X}_u, \mathbf{X}) = \sum_{u=1}^d \tilde{\alpha}_j(\mathbf{X}_u, \mathbf{X}) = 1$ by our assumption, we obtain

$$\sum_{q=1}^p \sum_{t=1}^T \frac{\partial g\{\mathbf{S}(\boldsymbol{\alpha})\}}{\partial S_{qt}(\boldsymbol{\alpha})} = \sum_{q=1}^p \sum_{t=1}^T \frac{\partial g\{\mathbf{S}(\tilde{\boldsymbol{\alpha}})\}}{\partial S_{qt}(\tilde{\boldsymbol{\alpha}})}.$$

And hence we have

$$\alpha_j(\mathbf{X}_u, \mathbf{X}) = \tilde{\alpha}_j(\mathbf{X}_u, \mathbf{X}), j = 1, \dots, p,$$

for any \mathbf{X} and any \mathbf{u} . Combined with (S1), this suggests

$$g\{\mathbf{S}(\boldsymbol{\alpha})\} = \tilde{g}\{\mathbf{S}(\boldsymbol{\alpha})\},$$

for all $\mathbf{X}_l, \mathbf{Z}_l$, which implies $g = \tilde{g}$. This contradicts with the assumption. Therefore, g and $\boldsymbol{\alpha}$ are identifiable.

S4 Proof of Lemma 1

Proof: First note that

$$\begin{aligned}\alpha_j(\mathbf{x}_l, \bar{\mathbf{x}}) - \alpha_{0j}(\mathbf{x}_l, \bar{\mathbf{x}}) &= \frac{\exp(\omega_j(\mathbf{x}_l))}{\sum_{l=1}^d \exp(\omega_j(\mathbf{x}_l))} - \frac{\exp(\omega_{0j}(\mathbf{x}_l))}{\sum_{l=1}^d \exp(\omega_{0j}(\mathbf{x}_l))} \\ &= \frac{\exp\{\omega_j^\dagger(\mathbf{x}_l)\}}{\sum_{l=1}^d \exp\{\omega_j^\dagger(\mathbf{x}_l)\}} \left\{ \left(1 - \frac{\exp(\omega_j^\dagger(\mathbf{x}_l))}{\sum_{l=1}^d \exp(\omega_j^\dagger(\mathbf{x}_l))} \right) \{\omega_j(\mathbf{x}_l) - \omega_{0j}(\mathbf{x}_l)\} \right. \\ &\quad \left. - \sum_{u \neq l} \frac{\exp(\omega_j^\dagger(\mathbf{x}_u))}{\sum_{l=1}^d \exp(\omega_j^\dagger(\mathbf{x}_l))} \{\omega_j(\mathbf{x}_u) - \omega_{0j}(\mathbf{x}_u)\} \right\},\end{aligned}$$

where ω_j^\dagger is one the line between ω_0 and ω_j , which implies

$$\sup_{\mathbf{x}_l, \mathbf{x}} |\alpha_j(\mathbf{x}_l, \mathbf{x}) - \alpha_{0j}(\mathbf{x}_l, \mathbf{x})| \leq 2 \sup_{\mathbf{x}_l} |\{\omega_j(\mathbf{x}_l) - \omega_{0j}(\mathbf{x}_l)\}|.$$

Furthermore,

$$\|\nabla g_0 \{\mathbf{S}_i(\boldsymbol{\alpha}_0)\}\|_2 \leq \|\mathbf{W}_{gL} \mathbf{W}_{gL-1}, \dots, \mathbf{W}_{g0}\|_2 \leq \sqrt{\prod_{l=1}^L s_{gl}},$$

where $\mathbf{W}_{gl}, l = 0, \dots, L$ are the weights for constructing g_0 , and s_{gl} is the sparseness of \mathbf{W}_{gl} . By the relationship between geometric and arithmetic means, we have $\prod_{l=1}^{L_g} s_{gl} \leq (\sum_{l=1}^{L_g} s_{gl}/L_g)^{L_g}$, which leads

$$\|\nabla g_0 \{\mathbf{S}_i(\boldsymbol{\alpha}_0)\}\|_2 \leq (s_g/L_g)^{L_g/2} \leq M_L. \quad (\text{S2})$$

The last inequality holds by Condition (C4). Moreover, because $\nabla_{j_t g_0} \{\mathbf{S}_i(\boldsymbol{\alpha}_0)\}$ has at most s_g nonzero elements,

$$\begin{aligned}& \left| \sum_{j=1}^p \sum_{t=1}^T \nabla_{j_t g_0} \{\mathbf{S}_i(\boldsymbol{\alpha}_0)\} \sum_{l=1}^d (X_{ilt} + Z_{ilj}) \{\alpha_j^*(\mathbf{X}_{il}, \mathbf{X}_i)^\top - \alpha_{j0}(\mathbf{X}_{il}, \mathbf{X}_i)^\top\} \right| \\ & \leq 2C_M M_L \sqrt{d \min(s_g, Tp)} \sup_{\mathbf{x}, j=1, \dots, p} |\alpha_j^*(\mathbf{x}_l, \mathbf{x}) - \alpha_{j0}(\mathbf{x}_l, \mathbf{x})|.\end{aligned}$$

Therefore, by Lemma S2, we have

$$\begin{aligned}& |h' [g^* \{\mathbf{S}_i(\boldsymbol{\alpha}^*)\}] - h' [g_0 \{\mathbf{S}_i(\boldsymbol{\alpha}_0)\}]| \\ &= |h'' [g^\dagger \{\mathbf{S}_i(\boldsymbol{\alpha}^\dagger)\}] [g^* \{\mathbf{S}_i(\boldsymbol{\alpha}_0)\} - g_0 \{\mathbf{S}_i(\boldsymbol{\alpha}_0)\}] + h'' [g^\dagger \{\mathbf{S}_i(\boldsymbol{\alpha}^\dagger)\}] \sum_{j=1}^p \sum_{t=1}^T \nabla_{j_t g^\dagger} \{\mathbf{S}_i(\boldsymbol{\alpha}^\dagger)\} \\ &\quad \times \sum_{l=1}^d (X_{ilt} + Z_{ilj}) \{\alpha_j^*(\mathbf{X}_{il}, \mathbf{X}_i)^\top - \alpha_{j0}(\mathbf{X}_{il}, \mathbf{X}_i)^\top\}| \\ &\leq \left\{ C_g \max_{u=0, \dots, q_g} c_g^{-\frac{\beta_{gu}^*}{t_{gu}}} n^{-\frac{\beta_{gu}^*}{2\beta_{gu}^* + t_{gu}}} + 2C_M M_L \sqrt{d \min(s_g, Tp)} \sup_{j=1, \dots, p} C_{\omega_j} \max_{u=0, \dots, q_{\omega_j}} c_{\omega_j}^{-\frac{\beta_{\omega_j u}^*}{t_{\omega_j u}}} n^{-\frac{\beta_{\omega_j u}^*}{2\beta_{\omega_j u}^* + t_{\omega_j u}}} \right\}.\end{aligned}$$

S5 Useful Lemmas for Theorem 1

Lemma S6 Let $\psi_{\hat{g}} = \hat{g} - g_0$ and $\psi_{\hat{\alpha}_j} = \hat{\alpha}_j - \alpha_{0j}$. Assume $\hat{\alpha}_j, \alpha_{0j} \in \mathcal{H}_j$, $\omega_j^* \in \mathcal{G}_{\omega_j}$, and $\hat{g}, g_0 \in \mathcal{F}_g$, and $g^* \in \mathcal{G}_g$ and Conditions (C1)–(C6) hold, and $T, p \leq s_g$. Then we have there are positive constants $C_g, C_{\omega_j}, c_g, c_{\omega_j}$, $\mathbf{C}_\omega = (C_{\omega_j}, j = 1, \dots, p)^\top$, $\mathbf{c}_\omega = (c_{\omega_j}, j = 1, \dots, p)^\top$ such that

$$\begin{aligned} & \left| n^{-1} \sum_{i=1}^n \left\{ (Y_i - h' [g_0 \{\mathbf{S}_i(\boldsymbol{\alpha}_0)\}]) \right. \right. \\ & \quad \left. \left. \sum_{j=1}^p \sum_{t=1}^T \nabla_{jt} g_0 \{\mathbf{S}_i(\boldsymbol{\alpha}_0)\} \sum_{l=1}^d (X_{ilt} + Z_{ilj}) \psi_{\hat{\alpha}_j}(\mathbf{X}_{il}, \mathbf{X}_i) \right\} \right| \\ & \leq 4C_M M_L \eta(C_g, \mathbf{C}_\omega, c_g, \mathbf{c}_\omega) \left(\left[dp E \left\{ \sum_{j=1}^p \sum_{l=1}^d \{\sqrt{T} \psi_{\hat{\alpha}_j}(\mathbf{X}_{il}, \mathbf{X}_i)\}^2 \right\} \right]^{1/2} \right. \\ & \quad \left. + \min(s_g, Tp)^{1/2} \{\log(n)/(cn)\}^{1/4} \right) \end{aligned}$$

with probability greater than $1 - 6n^{-1}$. And there are positive constants $B_g, B_{\omega_j}, b_g, b_{\omega_j}$, $\mathbf{B}_\omega = (B_{\omega_j}, j = 1, \dots, p)^\top$, $\mathbf{b}_\omega = (b_{\omega_j}, j = 1, \dots, p)^\top$ that

$$\begin{aligned} & \left| n^{-1} \sum_{i=1}^n \{ (Y_i - h' [g_0 \{\mathbf{S}_i(\boldsymbol{\alpha}_0)\}]) \psi_{\hat{g}} \{\mathbf{S}_i(\boldsymbol{\alpha}_0)\} \} \right| \\ & \leq 4C_M M_L \eta(B_g, B_g, \mathbf{B}_\omega, \mathbf{b}_\omega) \left[(E [\psi_{\hat{g}} \{\mathbf{S}_i(\boldsymbol{\alpha}_0)\}^2])^{1/2} + \{\log(n)/(cn)\}^{1/4} \right]. \end{aligned}$$

with probability greater than $1 - 6n^{-1}$.

Proof: Because $Y_i - h'[g^* \{\mathbf{S}_i(\boldsymbol{\alpha}^*)\}]$ is a sub-Gaussian random variable, by Lemma 1 that $|h'[g^* \{\mathbf{S}_i(\boldsymbol{\alpha}^*)\}] - h'[g_0 \{\mathbf{S}_i(\boldsymbol{\alpha}_0)\}]| \rightarrow 0$ almost surely, we have $Y_i - h'[g_0 \{\mathbf{S}_i(\boldsymbol{\alpha}_0)\}]$ is a sub-Gaussian random variable. Therefore using the concentration inequality in Lemma S4, we have

$$\begin{aligned} & \Pr \left[\left| n^{-1} \sum_{i=1}^n \{ (Y_i - h' [g_0 \{\mathbf{S}_i(\boldsymbol{\alpha}_0)\}]) - E(Y_i - h' [g_0 \{\mathbf{S}_i(\boldsymbol{\alpha}_0)\}] | \mathcal{X}_n) \} \right. \right. \\ & \quad \left. \left. \times \sum_{j=1}^p \sum_{t=1}^T \nabla_{jt} g_0 \{\mathbf{S}_i(\boldsymbol{\alpha}_0)\} \sum_{l=1}^d (X_{ilt} + Z_{ilj}) \psi_{\hat{\alpha}_j}(\mathbf{X}_{il}, \mathbf{X}_i) \right| \geq t \middle| \mathcal{X}_n \right] \\ & \leq 3 \exp \left(- \frac{nct^2}{16n^{-1} \sum_{i=1}^n \left[\sum_{j=1}^p \sum_{t=1}^T \nabla_{jt} g_0 \{\mathbf{S}_i(\boldsymbol{\alpha}_0)\} \sum_{l=1}^d (X_{ilt} + Z_{ilj}) \psi_{\hat{\alpha}_j}(\mathbf{X}_{il}, \mathbf{X}_i) \right]^2} \right). \end{aligned} \tag{S3}$$

Let

$$t = \sqrt{C_0 \log(n)/(cn)} \left(n^{-1} \sum_{i=1}^n \left[\sum_{j=1}^p \sum_{t=1}^T \nabla_{jt} g_0 \{ \mathbf{S}_i(\boldsymbol{\alpha}_0) \} \sum_{l=1}^d (X_{ilt} + Z_{ilj}) \psi_{\hat{\alpha}_j}(\mathbf{X}_{il}, \mathbf{X}_i) \right]^2 \right)^{1/2},$$

where $C_0 = 16$, we obtain

$$\begin{aligned} & \left| n^{-1} \sum_{i=1}^n \{ (Y_i - h' [g_0 \{ \mathbf{S}_i(\boldsymbol{\alpha}_0) \}]) - E(Y_i - h' [g_0 \{ \mathbf{S}_i(\boldsymbol{\alpha}_0) \}] | \mathcal{X}_n) \} \right. \\ & \quad \left. \sum_{j=1}^p \sum_{t=1}^T \nabla_{jt} g_0 \{ \mathbf{S}_i(\boldsymbol{\alpha}_0) \} \sum_{l=1}^d (X_{ilt} + Z_{ilj}) \psi_{\hat{\alpha}_j}(\mathbf{X}_{il}, \mathbf{X}_i) \right| \\ & \leq \sqrt{C_0 \log(n)/(cn)} \left(n^{-1} \sum_{i=1}^n \left[\sum_{j=1}^p \sum_{t=1}^T \nabla_{jt} g_0 \{ \mathbf{S}_i(\boldsymbol{\alpha}_0) \} \sum_{l=1}^d (X_{ilt} + Z_{ilj}) \psi_{\hat{\alpha}_j}(\mathbf{X}_{il}, \mathbf{X}_i) \right]^2 \right)^{1/2} \quad (\text{S4}) \end{aligned}$$

with probability greater than $1 - 3n^{-1}$.

Furthermore, Lemma 1 leads to

$$\begin{aligned} & \left| n^{-1} \sum_{i=1}^n E \{ (Y_i - h' [g_0 \{ \mathbf{S}_i(\boldsymbol{\alpha}_0) \}]) | \mathcal{X}_n \} \sum_{j=1}^p \sum_{t=1}^T \nabla_{jt} g_0 \{ \mathbf{S}_i(\boldsymbol{\alpha}_0) \} \sum_{l=1}^d (X_{ilt} + Z_{ilj}) \psi_{\hat{\alpha}_j}(\mathbf{X}_{il}, \mathbf{X}_i) \right| \\ & = \left| n^{-1} \sum_{i=1}^n \left\{ (h' [g^* \{ \mathbf{S}_i(\boldsymbol{\alpha}^*) \}] - h' [g_0 \{ \mathbf{S}_i(\boldsymbol{\alpha}_0) \}]) \right. \right. \\ & \quad \left. \left. \sum_{j=1}^p \sum_{t=1}^T \nabla_{jt} g_0 \{ \mathbf{S}_i(\boldsymbol{\alpha}_0) \} \sum_{l=1}^d (X_{ilt} + Z_{ilj}) \psi_{\hat{\alpha}_j}(\mathbf{X}_{il}, \mathbf{X}_i) \right\} \right| \\ & \leq \left\{ C_g \max_{u=0, \dots, q_g} c_g^{-\frac{\beta_{gu}^*}{t_{gu}}} n^{-\frac{\beta_{gu}^*}{2\beta_{gu}^* + t_{gu}}} + 2C_M M_L \sqrt{d \min(s_g, Tp)} \sup_{j=1, \dots, p} C_{\omega_j} \max_{u=0, \dots, q_{\omega_j}} c_{\omega_j}^{-\frac{\beta_{\omega_j u}^*}{t_{\omega_j u}}} n^{-\frac{\beta_{\omega_j u}^*}{2\beta_{\omega_j u}^* + t_{\omega_j u}}} \right\} \\ & \quad \left(n^{-1} \sum_{i=1}^n \left[\sum_{j=1}^p \sum_{t=1}^T \nabla_{jt} g_0 \{ \mathbf{S}_i(\boldsymbol{\alpha}_0) \} \sum_{l=1}^d (X_{ilt} + Z_{ilt}) \psi_{\hat{\alpha}_j}(\mathbf{X}_{il}, \mathbf{X}_i) \right]^2 \right)^{1/2}. \end{aligned}$$

Combine with (S4), we obtain there are positive constants $C_g, C_{\omega_j}, c_g, c_{\omega_j}$ such that

$$\begin{aligned} & \left| n^{-1} \sum_{i=1}^n \left\{ (Y_i - h' [g_0 \{ \mathbf{S}_i(\boldsymbol{\alpha}_0) \}]) \right. \right. \\ & \quad \left. \left. \sum_{j=1}^p \sum_{t=1}^T \nabla_{jt} g_0 \{ \mathbf{S}_i(\boldsymbol{\alpha}_0) \} \sum_{l=1}^d (X_{ilt} + Z_{ilj}) \psi_{\hat{\alpha}_j}(\mathbf{X}_{il}, \mathbf{X}_i) \right\} \right| \\ & \leq \eta(C_g, \mathbf{C}_\omega, c_g, \mathbf{c}_\omega) \left(n^{-1} \sum_{i=1}^n \left[\sum_{j=1}^p \sum_{t=1}^T \nabla_{jt} g_0 \{ \mathbf{S}_i(\boldsymbol{\alpha}_0) \} \sum_{l=1}^d (X_{ilt} + Z_{ilj}) \psi_{\hat{\alpha}_j}(\mathbf{X}_{il}, \mathbf{X}_i) \right]^2 \right)^{1/2} \quad (\text{S5}) \end{aligned}$$

with probability greater than $1 - 3n^{-1}$. Additionally, because $\sum_{l=1}^d \hat{\alpha}_j(\mathbf{x}_l, \mathbf{x}) = \sum_{l=1}^d \alpha_{0j}(\mathbf{x}_l, \mathbf{x}) = 1$, and $\nabla g_0 \{\mathbf{S}_i(\boldsymbol{\alpha}_0)\}$ is s_g sparse we have

$$\left| \sum_{j=1}^p \sum_{t=1}^T \nabla_{jt} g_0 \{\mathbf{S}_i(\boldsymbol{\alpha}_0)\} \sum_{l=1}^d (X_{ilt} + Z_{ilj}) \psi_{\hat{\alpha}_j}(\mathbf{X}_{il}, \mathbf{X}_i) \right| \leq 4C_M M_L \sqrt{\min(s_g, Tp)}.$$

Therefore $\left\{ \sum_{j=1}^p \sum_{t=1}^T \nabla_{jt} g_0 \{\mathbf{S}_i(\boldsymbol{\alpha}_0)\} \sum_{l=1}^d (X_{ilt} + Z_{ilj}) \psi_{\hat{\alpha}_j}(\mathbf{X}_{il}, \mathbf{X}_i) \right\}^2 / \min(s_g, Tp)$ is sub-Gaussian variable, and hence

$$\begin{aligned} & \Pr \left\{ \left| n^{-1} \min(s_g, Tp)^{-1} \sum_{i=1}^n \left[\sum_{j=1}^p \sum_{t=1}^T \nabla_{jt} g_0 \{\mathbf{S}_i(\boldsymbol{\alpha}_0)\} \sum_{l=1}^d (X_{ilt} + Z_{ilj}) \psi_{\hat{\alpha}_j}(\mathbf{X}_{il}, \mathbf{X}_i) \right]^2 \right. \right. \\ & \quad \left. \left. - \min(s_g, Tp)^{-1} E \left(\left[\sum_{j=1}^p \sum_{t=1}^T \nabla_{jt} g_0 \{\mathbf{S}_i(\boldsymbol{\alpha}_0)\} \sum_{l=1}^d (X_{ilt} + Z_{ilj}) \psi_{\hat{\alpha}_j}(\mathbf{X}_{il}, \mathbf{X}_i) \right]^2 \right) \right| > t \right\} \\ & \leq 3 \exp \left\{ -cnt^2 / (256C_M^4 M_L^4) \right\}. \end{aligned}$$

Let $t = \sqrt{256M_L^4 C_M^4 \log(n) / (cn)}$, we have

$$\begin{aligned} & \left| n^{-1} \sum_{i=1}^n \left\{ \sum_{j=1}^p \sum_{t=1}^T \nabla_{jt} g_0 \{\mathbf{S}_i(\boldsymbol{\alpha}_0)\} \sum_{l=1}^d (X_{ilt} + Z_{ilj}) \psi_{\hat{\alpha}_j}(\mathbf{X}_{il}, \mathbf{X}_i) \right\}^2 \right. \\ & \quad \left. - E \left(\left\{ \sum_{j=1}^p \sum_{t=1}^T \nabla_{jt} g_0 \{\mathbf{S}_i(\boldsymbol{\alpha}_0)\} \sum_{l=1}^d (X_{ilt} + Z_{ilj}) \psi_{\hat{\alpha}_j}(\mathbf{X}_{il}, \mathbf{X}_i) \right\}^2 \right) \right| \\ & \leq 16 \min(s_g, Tp) C_M^2 M_L^2 \sqrt{\log(n) / (cn)}, \end{aligned} \tag{S6}$$

with probability greater than $1 - 3/n$. Next

$$\begin{aligned} & E \left(\left[\sum_{j=1}^p \sum_{t=1}^T \nabla_{jt} g_0 \{\mathbf{S}_i(\boldsymbol{\alpha}_0)\} \sum_{l=1}^d (X_{ilt} + Z_{ilj}) \psi_{\hat{\alpha}_j}(\mathbf{X}_{il}, \mathbf{X}_i) \right]^2 \right) \\ & \leq E \left(\left[\sup_{l=1, \dots, d, j=1, \dots, p} \sum_{t=1}^T \nabla_{jt} g_0 \{\mathbf{S}_i(\boldsymbol{\alpha}_0)\} (X_{ilt} + Z_{ilj}) / \sqrt{T} \left| \sum_{j=1}^p \sum_{l=1}^d |\sqrt{T} \psi_{\hat{\alpha}_j}(\mathbf{X}_{il}, \mathbf{X}_i)| \right| \right]^2 \right) \\ & \leq 4C_M^2 M_L^2 E \left\{ \left(\sqrt{dp} \left[\sum_{j=1}^p \sum_{l=1}^d \left\{ \sqrt{T} \psi_{\hat{\alpha}_j}(\mathbf{X}_{il}, \mathbf{X}_i) \right\}^2 \right]^{1/2} \right)^2 \right\} \\ & = 4C_M^2 M_L^2 dp E \left[\sum_{j=1}^p \sum_{l=1}^d \left\{ \sqrt{T} \psi_{\hat{\alpha}_j}(\mathbf{X}_{il}, \mathbf{X}_i) \right\}^2 \right], \end{aligned}$$

for a constant C_M , where the second inequality holds because

$$\begin{aligned}
& \left| \sup_{l=1, \dots, d, j=1, \dots, p} \sum_{t=1}^T \nabla_{jt} g_0 \{ \mathbf{S}_i(\boldsymbol{\alpha}_0) \} (X_{ilt} + Z_{ilj}) \right| \\
& \leq 2C_M \sup_{l=1, \dots, d, j=1, \dots, p} \sum_{t=1}^T |\nabla_{jt} g_0 \{ \mathbf{S}_i(\boldsymbol{\alpha}_0) \}| \\
& \leq 2C_M \sqrt{T} \sup_{l=1, \dots, d, j=1, \dots, p} \left[\sum_{t=1}^T |\nabla_{jt} g_0 \{ \mathbf{S}_i(\boldsymbol{\alpha}_0) \}| \right]^{1/2} \\
& \leq 2C_M \sqrt{T} M_L,
\end{aligned}$$

by (S2). Plugging the above inequality and (S6) to (S5), we obtain

$$\begin{aligned}
& \left| n^{-1} \sum_{i=1}^n \{ (Y_i - h' [g_0 \{ \mathbf{S}_i(\boldsymbol{\alpha}_0) \}]) \right. \\
& \quad \left. \sum_{j=1}^p \sum_{t=1}^T \nabla_j g_0 \{ \mathbf{S}_i(\boldsymbol{\alpha}_0) \} \sum_{l=1}^d (X_{ilt} + Z_{ilj}) \psi_{\hat{\alpha}_j}(\mathbf{X}_{il}, \mathbf{X}_i) \right\} \Big| \\
& \leq \eta(C_g, \mathbf{C}_\omega, c_g, \mathbf{c}_\omega) \left(2C_M M_L \left[dp E \left\{ \sum_{j=1}^p \sum_{l=1}^d \{ \sqrt{T} \psi_{\hat{\alpha}_j}(\mathbf{X}_{il}, \mathbf{X}_i) \}^2 \right\} \right]^{1/2} \right. \\
& \quad \left. + 4C_M M_L \min(s_g, Tp)^{1/2} \{ \log(n)/(cn) \}^{1/4} \right) \\
& \leq 4C_M M_L \eta(C_g, \mathbf{C}_\omega, c_g, \mathbf{c}_\omega) \left(\left[dp E \left\{ \sum_{j=1}^p \sum_{l=1}^d \{ \sqrt{T} \psi_{\hat{\alpha}_j}(\mathbf{X}_{il}, \mathbf{X}_i) \}^2 \right\} \right]^{1/2} \right. \\
& \quad \left. + \min(s_g, Tp)^{1/2} \{ \log(n)/(cn) \}^{1/4} \right)
\end{aligned}$$

with probability greater than $1 - 6n^{-1}$. Using the same arguments and realize that we obtain there are positive constants $B_g, B_{\omega_j}, b_g, b_{\omega_j}$ and realize that $\|\psi_{\hat{g}}\|_2 \leq 2C_M M_L$, we have

$$\begin{aligned}
& \left| n^{-1} \sum_{i=1}^n \{ (Y_i - h' [g_0 \{ \mathbf{S}_i(\boldsymbol{\alpha}_0) \}]) \psi_{\hat{g}} \{ \mathbf{S}_i(\boldsymbol{\alpha}_0) \} \} \right| \\
& \leq 4C_M M_L \eta(B_g, \mathbf{B}_\omega, b_g, \mathbf{B}_\omega) \left[(E [\psi_{\hat{g}} \{ \mathbf{S}_i(\boldsymbol{\alpha}_0) \}^2])^{1/2} + \{ \log(n)/(cn) \}^{1/4} \right].
\end{aligned}$$

with probability greater than $1 - 6n^{-1}$. This proves the result.

Lemma S7 Assume $\hat{\alpha}_j, \alpha_{0j} \in \mathcal{H}_j$, $\omega_j^* \in \mathcal{G}_{\omega_j}$, and $\hat{g}, g_0 \in \mathcal{F}_g$, $g^* \in \mathcal{G}_g$. Furthermore, assume Condition (C1)–(C7) hold, and $d/n \rightarrow 0$ and $T/n \rightarrow 0$ and $p < \infty$. Then for given

$\epsilon_g^\dagger, \epsilon_{\alpha_j}^\dagger \in (0, 1)$, $\epsilon_\alpha^\dagger = \{\epsilon_{\alpha_j}^\dagger, j = 1, \dots, p\}^\top$, we have

$$\begin{aligned} \Omega(g_0, \alpha_0, \psi_{\hat{g}}, \psi_{\hat{\alpha}}, \epsilon_g^\dagger, \epsilon_\alpha^\dagger) &\geq \alpha_{\min} E \left[\psi_{\hat{g}} \{ \mathbf{S}_i(\alpha_0) \}^2 + \sum_{j=1}^p \sum_{l=1}^d T \psi_{\hat{\alpha}_j}(\mathbf{X}_{il}, \mathbf{X}_i)^2 \right] \\ &\quad - 2TpC_1 \log^2(n) \left\{ \phi_{gn} L_g + \sum_{j=1}^p \phi_{\omega_j n} L_{\omega_j} \right\} - C_H Tp/n \end{aligned}$$

with probability greater than $1 - 2 \exp \left[-nC_1 \log^2(n) \left\{ \phi_{gn} L_g + \sum_{j=1}^p \phi_{\omega_j n} L_{\omega_j} \right\} \right]$ for some constants $C_H, C_1 > 0$.

Proof: Let $\psi_{\hat{g}} = \hat{g} - g_0$, $\psi_{\hat{\alpha}_k} = \hat{\alpha}_k - \alpha_0$. First, because $\hat{g}, g_0, \hat{\alpha}_k, \alpha_0$ are bounded functions, ∇g is bounded in the sense of S2, and Y_i is bounded, and $\|\mathbf{X}_{il}\|_2 \leq C_M \sqrt{T}$ by Condition (C5), it is easy to see that every summand in $Tp^{-1} \Omega(g_0, \alpha_0, \psi_g, \psi_\alpha, \epsilon_g^\dagger, \epsilon_\alpha^\dagger)$ is a product of bounded sub-Gaussian variable, and hence sub-exponential. Therefore, by Lemma S5, for arbitrary g, α , there is a constant $c_H > 0$ such that

$$\begin{aligned} &\Pr \left\{ |(Tp)^{-1} \Omega(g_0, \alpha_0, \psi_g, \psi_\alpha, \epsilon_g^\dagger, \epsilon_\alpha^\dagger) - (Tp)^{-1} E \{ \Omega(g_0, \alpha_0, \psi_g, \psi_\alpha, \epsilon_g^\dagger, \epsilon_\alpha^\dagger) \}| > t \right\} \\ &\leq 3 \exp \{ -c_H n \min(t^2, t) \}. \end{aligned}$$

Let $\mathcal{S}_g(\delta)$ be the δ covering of \mathcal{F}_g and $\mathcal{S}_{\omega_k}(\delta)$ be the δ covering of \mathcal{F}_{ω_k} , then for some constant $C_H > 0$, we have

$$\begin{aligned} &\Pr \left\{ \sup_{g \in \mathcal{F}_g, \alpha_k \in \mathcal{H}_k} |\Omega(g_0, \alpha_0, \psi_g, \psi_\alpha, \epsilon_g^\dagger, \epsilon_\alpha^\dagger) - E \{ \Omega(g_0, \alpha_0, \psi_g, \psi_\alpha, \epsilon_g^\dagger, \epsilon_\alpha^\dagger) \}| > Tpt + C_H Tp\delta \right\} \\ &\leq \Pr \left\{ \max_{g \in \mathcal{S}_g, \omega_k \in \mathcal{S}_{\omega_k}} |\Omega(g_0, \alpha_0, \psi_g, \psi_\alpha, \epsilon_g^\dagger, \epsilon_\alpha^\dagger) - E \{ \Omega(g_0, \alpha_0, \psi_g, \psi_\alpha, \epsilon_g^\dagger, \epsilon_\alpha^\dagger) \}| > Tpt \right\} \\ &\leq 2 \exp \left[-c_H n \min(t^2, t) + \log \mathcal{N} \{ \delta, \mathcal{F}_g, \|\cdot\|_\infty \} + \sum_{k=1}^p \log \mathcal{N} \{ \delta, \mathcal{F}_{\omega_k}, \|\cdot\|_\infty \} \right] \\ &\leq 2 \exp \left[-c_H n \min(t^2, t) + (s_g + 1) \log \left\{ 2^{2L_g+5} \delta^{-1} (L+1) p_{g0}^2 p_{gL_g+1}^2 s_g^{2L_g} \right\} \right. \\ &\quad \left. + \sum_{k=1}^p (s_{\omega_k} + 1) \log \left\{ 2^{2L_{\omega_k}+5} \delta^{-1} (L\omega_k + 1) p_{\omega_k 0}^2 p_{\omega_k L_{\omega_k}+1}^2 s_{\omega_k}^{2L_{\omega_k}} \right\} \right] \\ &\leq 2 \exp \left[-c_H n \min(t^2, t) + (s_g + 1) L_g \log \left\{ 2s_g \delta^{-1} (L_g + 1) d^2 p^2 s_g^{2L_g} \right\} \right. \\ &\quad \left. + \sum_{k=1}^p (s_{\omega_k} + 1) \log \left\{ 2^{2L_{\omega_k}+5} \delta^{-1} (L\omega_k + 1) p_{\omega_k 0}^2 p_{\omega_k L_{\omega_k}+1}^2 s_{\omega_k}^{2L_{\omega_k}} \right\} \right] \end{aligned}$$

Now plugging $\delta = n^{-1}$ using Condition (C2)–(C4) and the fact that $d/n \rightarrow 0$ and $T/n \rightarrow 0$

and $p < \infty$, we have

$$\begin{aligned} & \Pr \left\{ \sup_{g \in \mathcal{F}_g, \alpha_k \in \mathcal{H}_k} |\Omega(g_0, \boldsymbol{\alpha}_0, \psi_g, \boldsymbol{\psi}_\alpha, \epsilon_g^\dagger, \epsilon_\alpha^\dagger) - E\{\Omega(g_0, \boldsymbol{\alpha}_0, \psi_g, \boldsymbol{\psi}_\alpha, \epsilon_g^\dagger, \epsilon_\alpha^\dagger)\}| > Tpt + C_H Tp/n \right\} \\ & \leq 2 \exp \left[-c_H n \min(t^2, t) + c_1 n \phi_{gn} L_g \log^2(n) + \sum_{j=1}^p c_{2j} n \phi_{\omega_j n} L_{\omega_j} \log^2(n) \right]. \end{aligned}$$

Let $t = \max \left[2C_1 \log^2(n) \left\{ \phi_{gn} L_g + \sum_{j=1}^p \phi_{\omega_j n} L_{\omega_j} \log^2(n) \right\}, 1 \right]$, where $C_1 = 2\{c_1 + \max_j(c_{2j})\}/c_H$, we have

$$\begin{aligned} & \Pr \left\{ \sup_{g \in \mathcal{F}_g, \alpha_k \in \mathcal{H}_k} |\Omega(g_0, \boldsymbol{\alpha}_0, \psi_g, \boldsymbol{\psi}_\alpha, \epsilon_g^\dagger, \epsilon_\alpha^\dagger) - E\{\Omega(g_0, \boldsymbol{\alpha}_0, \psi_g, \boldsymbol{\psi}_\alpha, \epsilon_g^\dagger, \epsilon_\alpha^\dagger)\}| \right. \\ & > 2TpC_1 \log^2(n) \left\{ \phi_{gn} L_g + \sum_{j=1}^p \phi_{\omega_j n} L_{\omega_j} \right\} + C_H Tp/n \left. \right\} \\ & \leq 2 \exp \left[-nC_1 \log^2(n) \left\{ \phi_{gn} L_g + \sum_{j=1}^p \phi_{\omega_j n} L_{\omega_j} \right\} \right]. \end{aligned}$$

Therefore,

$$\begin{aligned} & |\Omega(g_0, \boldsymbol{\alpha}_0, \psi_{\hat{g}}, \boldsymbol{\psi}_{\hat{\alpha}}, \epsilon_g^\dagger, \epsilon_\alpha^\dagger) - E\{\Omega(g_0, \boldsymbol{\alpha}_0, \psi_{\hat{g}}, \boldsymbol{\psi}_{\hat{\alpha}}, \epsilon_g^\dagger, \epsilon_\alpha^\dagger)\}| \\ & \leq TpC_1 \log^2(n) \left\{ \phi_{gn} L_g + \sum_{j=1}^p \phi_{\omega_j n} L_{\omega_j} \right\} + C_H Tp/n, \end{aligned}$$

with probability greater than $1 - 2 \exp \left[-nC_1 \log^2(n) \left\{ \phi_{gn} L_g + \sum_{j=1}^p \phi_{\omega_j n} L_{\omega_j} \right\} \right]$ for some $C_1 > 0$. Hence

$$\begin{aligned} & \Omega(g_0, \boldsymbol{\alpha}_0, \psi_{\hat{g}}, \boldsymbol{\psi}_{\hat{\alpha}}, \epsilon_g^\dagger, \epsilon_\alpha^\dagger) \geq \alpha_{\min} E \left[\psi_{\hat{g}} \{ \mathbf{S}_i(\boldsymbol{\alpha}_0) \}^2 + \sum_{j=1}^p \sum_{l=1}^d T \psi_{\hat{\alpha}_j}(\mathbf{X}_{il}, \mathbf{X}_i)^2 \right] \\ & - TpC_1 \log^2(n) \left\{ \phi_{gn} L_g + \sum_{j=1}^p \phi_{\omega_j n} L_{\omega_j} \right\} - C_H Tp/n \end{aligned}$$

with probability greater than $1 - 2 \exp \left[-nC_1 \log^2(n) \left\{ \phi_{gn} L_g + \sum_{j=1}^p \phi_{\omega_j n} L_{\omega_j} \right\} \right]$. This proves the result.

S6 Proof of Theorem 1

Proof: Because \widehat{g} , $\widehat{\alpha}$ is the minimizer of (4), we have

$$\begin{aligned}
0 &\geq \mathcal{L}(\widehat{g}, \widehat{\alpha}) - \mathcal{L}(g_0, \alpha_0) \\
&= -n^{-1} \sum_{i=1}^n \left\{ (Y_i - h' [g_0 \{ \mathbf{S}_i(\alpha_0) \}]) \right. \\
&\quad \left. \sum_{j=1}^p \sum_{t=1}^T \nabla_{jt} g_0 \{ \mathbf{S}_i(\alpha_0) \} \sum_{l=1}^d (X_{ilt} + Z_{ilj}) \psi_{\widehat{\alpha}_j}(\mathbf{X}_{il}, \mathbf{X}_i) \right\} \\
&\quad - n^{-1} \sum_{i=1}^n [(Y_i - h' [g_0 \{ \mathbf{S}_i(\alpha_0) \}]) \psi_{\widehat{g}} \{ \mathbf{S}_i(\alpha_0) \}] \\
&\quad + \Omega(g_0, \alpha_0, \psi_{\widehat{g}}, \psi_{\widehat{\alpha}}, \epsilon_g^\dagger, \epsilon_\alpha^\dagger) / 2,
\end{aligned}$$

where $\epsilon_g^\dagger, \epsilon_\alpha^\dagger \in (0, 1)$ and $\epsilon_\alpha^\dagger = (\epsilon_{\alpha_j}^\dagger, j = 1, \dots, p)^\top$. By Lemma S6 and S7, we have there are positive constants $D_g, d_g, \mathbf{D}_\omega = (D_{\omega_j}), \mathbf{d}_\omega = (d_{\omega_j})$ such that

$$\begin{aligned}
&4C_M M_L \eta(D_g, d_g, \mathbf{D}_\omega, \mathbf{d}_\omega) \left[\left[dp E \left\{ \sum_{j=1}^p \sum_{l=1}^d T \psi_{\widehat{\alpha}_j}(\mathbf{X}_{il}, \mathbf{X}_i)^2 \right\} \right]^{1/2} + (E [\psi_{\widehat{g}} \{ \mathbf{S}_i(\alpha_0) \}^2])^{1/2} \right] \\
&+ 4C_M M_L \eta(D_g, d_g, \mathbf{D}_\omega, \mathbf{d}_\omega) \left[\min(s_g, Tp)^{1/2} \{ \log(n)/(cn) \}^{1/4} + \{ \log(n)/(cn) \}^{1/4} \right] \\
&+ Tp C_1 \log^2(n) \left\{ \phi_{gn} L_g + \sum_{j=1}^p \phi_{\omega_j n} L_{\omega_j} \right\} / 2 + C_H Tp / (2n) \\
&\geq \alpha_{\min} E \left[\psi_{\widehat{g}} \{ \mathbf{S}_i(\alpha_0) \}^2 + \sum_{j=1}^p \sum_{l=1}^d T \psi_{\widehat{\alpha}_j}(\mathbf{X}_{il}, \mathbf{X}_i)^2 \right] / 2
\end{aligned}$$

with probability greater than $1 - 6n^{-1} - 2 \exp \left[-nC_1 \log^2(n) \left\{ \phi_{gn} L_g + \sum_{j=1}^p \phi_{\omega_j n} L_{\omega_j} \right\} \right]$. This implies

$$\begin{aligned}
&4C_M M_L \eta(D_g, d_g, \mathbf{D}_\omega, \mathbf{d}_\omega) (dp/2)^{1/2} \left(E \left\{ \sum_{j=1}^p \sum_{l=1}^d T \psi_{\widehat{\alpha}_j}(\mathbf{X}_{il}, \mathbf{X}_i)^2 \right\} \right. \\
&\quad \left. + E [\psi_{\widehat{g}} \{ \mathbf{S}_i(\alpha_0) \}^2] \right)^{1/2} \\
&+ 4C_M M_L \eta(D_g, d_g, \mathbf{D}_\omega, \mathbf{d}_\omega) \left[\min(s_g, Tp)^{1/2} \{ \log(n)/(cn) \}^{1/4} + \{ 16 \log(n)/(cn) \}^{1/4} \right] \\
&+ Tp C_1 \log^2(n) \left\{ \phi_{gn} L_g + \sum_{j=1}^p \phi_{\omega_j n} L_{\omega_j} \right\} / 2 + C_H Tp / (2n) \\
&\geq \alpha_{\min} E \left[\psi_{\widehat{g}} \{ \mathbf{S}_i(\alpha_0) \}^2 + \sum_{j=1}^p \sum_{l=1}^d T \psi_{\widehat{\alpha}_j}(\mathbf{X}_{il}, \mathbf{X}_i)^2 \right] / 2.
\end{aligned}$$

Therefore, we have

$$\begin{aligned}
& E \left[\psi_{\hat{g}} \{ \mathbf{S}_i(\boldsymbol{\alpha}_0) \}^2 + \sum_{j=1}^p \sum_{l=1}^d T \psi_{\hat{\alpha}_j}(\mathbf{X}_{il}, \mathbf{X}_i)^2 \right] \\
& \leq 16\alpha_{\min}^{-1} \left(C_M M_L \eta(D_g, d_g, \mathbf{D}_\omega, \mathbf{d}_\omega) \left[\min(s_g, Tp)^{1/2} \{ \log(n)/(cn) \}^{1/4} + \{ \log(n)/(cn) \}^{1/4} \right] \right. \\
& \quad \left. + Tp C_1 \log^2(n) \left\{ \phi_{gn} L_g + \sum_{j=1}^p \phi_{\omega_j n} L_{\omega_j} \right\} / 2 + C_H T p / (2n) \right) \\
& \quad + 32 C_M M_L d p \alpha_{\min}^{-2} \eta(D_g, d_g, \mathbf{D}_\omega, \mathbf{d}_\omega)^2.
\end{aligned}$$

Now because $\|dP_{\boldsymbol{\alpha}_0}(\mathbf{z})/dP_{\boldsymbol{\alpha}^*}(\mathbf{z})\|_\infty \geq m_h$ almost surely, we obtain

$$\begin{aligned}
& E \left[\psi_{\hat{g}} \{ \mathbf{S}_i(\boldsymbol{\alpha}^*) \}^2 + \sum_{j=1}^p \sum_{l=1}^d T \psi_{\hat{\alpha}_j}(\mathbf{X}_{il}, \mathbf{X}_i)^2 \right] \\
& \leq 16 \min(m_h, 1)^{-1} \alpha_{\min}^{-1} \left(C_M M_L \eta(D_g, d_g, \mathbf{D}_\omega, \mathbf{d}_\omega) \left[\min(s_g, Tp)^{1/2} \{ \log(n)/(cn) \}^{1/4} + \{ \log(n)/(cn) \}^{1/4} \right] \right. \\
& \quad \left. + Tp C_1 \log^2(n) \left\{ \phi_{gn} L_g + \sum_{j=1}^p \phi_{\omega_j n} L_{\omega_j} \right\} + C_H T p / n \right) \\
& \quad + 32 \min(m_h, 1)^{-1} C_M M_L d p \alpha_{\min}^{-2} \eta(D_g, d_g, \mathbf{D}_\omega, \mathbf{d}_\omega)^2.
\end{aligned}$$

Now again using Lemma S2, we obtain there are constants D_{g1}, D_{ω_j1} such that

$$\begin{aligned}
& \int \{ \hat{g}(\mathbf{z}) - g^*(\mathbf{z}) \}^2 dP_{\boldsymbol{\alpha}^*}(\mathbf{z}) + T \sum_{j=1}^p \int \sum_{l=1}^d \{ \hat{\alpha}_j(\mathbf{x}_l, \mathbf{x}) - \alpha_j^*(\mathbf{x}_l, \mathbf{x}) \}^2 dP_{\mathbf{X}}(\mathbf{x}) \\
& \leq 16 \min(m_h, 1)^{-1} \alpha_{\min}^{-1} \left(C_M M_L \eta(D_g, d_g, \mathbf{D}_\omega, \mathbf{d}_\omega) \left[\min(s_g, Tp)^{1/2} \{ \log(n)/(cn) \}^{1/4} + \{ \log(n)/(cn) \}^{1/4} \right] \right. \\
& \quad \left. + Tp C_1 \log^2(n) \left\{ \phi_{gn} L_g + \sum_{j=1}^p \phi_{\omega_j n} L_{\omega_j} \right\} + C_H T p / n \right) \\
& \quad + 32 \min(m_h, 1)^{-1} C_M M_L d p \alpha_{\min}^{-2} \eta(D_g, d_g, \mathbf{D}_\omega, \mathbf{d}_\omega)^2 + \left(D_{g1} \phi_{gn} + T \sum_{j=1}^p D_{\omega_j1} \phi_{\omega_j n} \right)
\end{aligned}$$

with probability greater than $1 - 6n^{-1} - 2 \exp \left[-n C_1 \log^2(n) \left\{ \phi_{gn} L_g + \sum_{j=1}^p \phi_{\omega_j n} L_{\omega_j} \right\} \right]$.

This proves the result.

S7 The Standard ACNS Temporal Central Parasagittal (TCP) Montage

Table S1: The standard ACNS TCP montage.

Index	Montage	Anode	Cathode
0	FP1-F7	EEG FP1-REF	EEG F7-REF
1	F7-T3	EEG F7-REF	EEG T3-REF
2	T3-T5	EEG T3-REF	EEG T5-REF
3	T5-O1	EEG T5-REF	EEG O1-REF
4	FP2-F8	EEG FP2-REF	EEG F8-REF
5	F8-T4	EEG F8-REF	EEG T4-REF
6	T4-T6	EEG T4-REF	EEG T6-REF
7	T6-O2	EEG T6-REF	EEG O2-REF
8	A1-T3	EEG A1-REF	EEG T3-REF
9	T3-C3	EEG T3-REF	EEG C3-REF
10	C3-CZ	EEG C3-REF	EEG CZ-REF
11	CZ-C4	EEG CZ-REF	EEG C4-REF
12	C4-T4	EEG C4-REF	EEG T4-REF
13	T4-A2	EEG T4-REF	EEG A2-REF
14	FP1-F3	EEG FP1-REF	EEG F3-REF
15	F3-C3	EEG F3-REF	EEG C3-REF
16	C3-P3	EEG C3-REF	EEG P3-REF
17	P3-O1	EEG P3-REF	EEG O1-REF
18	FP2-F4	EEG FP2-REF	EEG F4-REF
19	F4-C4	EEG F4-REF	EEG C4-REF
20	C4-P4	EEG C4-REF	EEG P4-REF
21	P4-O2	EEG P4-REF	EEG O2-REF